Environmental Fluid Mechanics (2019) 19:81–109
https://doi.org/10.1007/s10652-018-9606-8

ORIGINAL ARTICLE

Flow and temperature dynamics in an urban canyon under a comprehensive set of wind directions, wind speeds, and thermal stability conditions

A. A. Aliabadi[1] · M. Moradi[2] · D. Clement[2] · W. D. Lubitz[2] · B. Gharabaghi[2]

Received: 21 November 2017 / Accepted: 5 June 2018 / Published online: 15 June 2018

Abstract
Atmospheric flow and temperature dynamics in the urban roughness sublayer exhibit numerous complexities that cannot all be investigated using models or scaled-down experiments, thus these complexities necessitate careful field observations. Such dynamics were studied under a comprehensive set of wind directions, wind speeds, and thermal stability conditions in a field campaign held in Guelph, Ontario, Canada, from 13th to 25th of August 2017. The urban site was a quasi-two-dimensional canyon with unit canyon aspect ratio. Beside characterizing thermal stability, inertial effects, urban heat island intensity, and mean properties of the atmosphere, the turbulence statistics were studied carefully as functions of roof-level wind angle, diurnal time, the building Reynolds number, or the bulk Richardson number. Turbulence statistics in the vertical direction were observed to be influenced by local conditions, such as flow properties and nearby surface temperatures. These statistics also indicated presence of small integral lengthscales and short integral timescales. On the other hand, turbulence statistics in the horizontal directions were influenced by non-local conditions, such as horizontal heterogeneity in heating or urban morphology. These statistics indicated presence of large integral lengthscales and long integral timescales. In addition, a rigorous scaling analysis was performed to seek significant correlations between turbulence statistics and other known flow variables both locally or as measured at a nearby non-urban rural station. Variances scaled more successfully to mean quantities than covariances (Reynolds stresses and turbulence kinematic heat fluxes). In addition, the statistics in the vertical direction scaled more successfully compared to horizontal directions. Statistics in the horizontal directions, particularly in the along-canyon axis direction, were poorly scaled, suggesting presence of unorganized and irregular turbulence structures influenced by non-local conditions. Temperature difference between the atmosphere and nearby surfaces as well as measured velocity scales showed to scale vertical heat fluxes successfully.

Keywords Scaling · Turbulence statistics · Urban boundary layer · Urban climate

✉ A. A. Aliabadi
aliabadi@uoguelph.ca

[1] Atmospheric Innovations Research (AIR) Laboratory, Environmental Engineering, School of Engineering, RICH 2515, University of Guelph, Guelph, ON, N1G 2W1, Canada

[2] School of Engineering, University of Guelph, Guelph, ON, N1G 2W1, Canada

1 Introduction

It has been suggested that flow and temperature dynamics in the urban environment exhibit numerous complexities in contrast to simpler conditions observed in rural areas or simplified wind tunnel or water channel experiments. Such dynamic complexities are pronounced in the urban roughness sublayer (RSL), where individual roughness elements such as buildings and vegetation have a direct effect on flow properties [39]. In the simplest urban morphologies, such as those found in regular two-dimensional canyons with cross-flow conditions, flows exhibit the isolated roughness, wake interference, or skimming regimes, depending on the spacing of buildings relative to the characteristic length of the buildings [36]. More complex dynamics arise with unequal building heights, altered roofs, differential surface temperatures, approach flow thermal stability, vegetation, oblique wind angles, non-regular morphologies, and three-dimensional effects (e.g. caused by intersections) [3–7, 9–11, 15, 19, 21, 22, 28, 29, 32, 33, 38, 40, 41, 49]. In the subsequent brief literature review, the majority of the studies reported are focused on urban microclimate field campaigns, while only a few scaled-down experiments, using wind tunnels, or simulation studies are reported, mainly to provide the context for the topics discussed.

Numerous studies have focused on flow dynamics in urban canyons. The effect of varying roof-level wind angle and wind velocity on flow dynamics within urban canyons have been reported to be significant. When approach flow is perpendicular to a long canyon, a single vortex with rotation axis parallel to the canyon axis is formed [5, 11, 21, 49]. On the other hand, around the edges of a canyon, such as in the street intersections, both horizontal and vertical vortices have been found [21, 49]. Flow channeling within canyons has been observed when approaching wind angles change toward the canyon axis [11, 21] and even more surprisingly with cross-wind directions [21, 22]. It has been suggested that oblique wind angles create combinations of flow channelling and recirculation within the canyon [21]. In addition, the presence of intersections, non-regular urban morphology, deep canyons, and short-term background wind variations created highly transient and three-dimensional flow patterns inside the canyon [5, 11, 32]. The single steady vortex in two-dimensional canyons with cross-flow has been reported to diminish with reducing wind velocities. Under such low wind conditions, multiple transient and short-lived vortices have been observed [11, 22]. Complexities in the urban morphology, such as the use of pitched roofs as opposed to flat roofs, have been reported to increase large, non-localized, and intermittent turbulence events [19–21, 28, 32].

Numerous studies have focused on temperature and heat dynamics in urban canyons. Thermal stability in urban microclimate field campaigns has been defined in various ways. A common method is to use the bulk Richardson number in the vertical direction $Ri_b = gH\Delta\overline{T}/((\Delta\overline{S})^2\overline{T}_A)$, where g is gravitational acceleration, H is building height, $\Delta\overline{T}$ is change in temperature over vertical distance H, $\Delta\overline{S}$ is change in horizontal wind speed, and $\overline{T}_A$ is average ambient temperature [6, 22, 26, 27]. The bulk Richardson number has also been defined in the horizontal direction such that $Ri_h = gH^2\Delta\overline{T}/((\Delta\overline{S})^2\overline{T}_A W)$, where now $\Delta\overline{T}$ is the horizontal temperature difference over the width of the urban canyon W [30, 31]. Alternatively, thermal stability in urban microclimate field campaigns can be defined using the stability parameter z/L, where z is height above ground and $L = -u_*^3\overline{T}/(\kappa g\overline{w'T'})$ is the Monin–Obukhov lengthscale [12, 16, 17, 21, 32, 33, 38, 49]. Here $u_* = (\overline{u'w'}^2 + \overline{v'w'}^2)^{1/4}$ is friction velocity with u', v', and w' showing the velocity fluctuations in the x, y, and z directions, respectively, T is a reference temperature, κ is the von Kármán constant, and T' is temperature fluctuation. The overbar notation signifies a time average. Some studies

report a strong dependence of turbulence statistics and heat transfer on atmospheric stability [27, 40]. Other studies report such dependence only based on the height chosen for the scaling variables [21] or for the energy-related turbulence statistics such as temperature or turbulence kinematic heat fluxes [38]. It has been suggested that the effect of thermal stability on the urban microclimate is determined by non-local spatiotemporal features of the atmosphere involving complex interactions among boundary layer development over both rural and urban locations over many hours, mixing height, surface heat fluxes, and nocturnal jets [6]. Some studies have reported microscale spatial variability in air temperature in the urban environment under various thermal stability conditions as measured by different weather stations installed in neighbouring areas [10, 15]. There is general consensus that greening of the urban environment has a net cooling effect on the urban microclimate, although the climatic conditions, types of vegetation, and urban planning must be performed carefully to maximize the cooling benefits [18].

Numerous scaling variables have been used to seek statistical correlations with turbulence parameters. Commonly used scaling variables are building height H, average wind speed $\overline{S}$, average velocity in the x direction $\overline{U}$, average velocity in the y direction $\overline{V}$, and friction velocity u_* at some reference location [5, 7, 8, 16, 20–22, 28, 33, 38]. Less commonly used scaling variables are the convective velocity scale $w_* = (gz_i\overline{w'T'}/T)^{1/3}$ and heat flux in the vertical direction $T_* = \overline{w'T'}$ at some reference location z_i [6, 14, 37, 49]. The reference height for the scaling variables has been reported to influence scaling of turbulence statistics significantly [21, 22].

Microclimate field studies that attempt to investigate flow and temperature dynamics in and around an urban canyon environment are limited in various aspects. Multiple studies have focused on describing momentum dynamics in detail, including the investigation of spectral properties of turbulence, while they leave the detailed analysis of temperature dynamics and thermal stability, for instance transport of turbulence heat fluxes, for future work [5, 7, 16, 32, 33]. Even some studies that focus solely on momentum dynamics do not report observations associated with a comprehensive set of wind angles [7, 11, 12, 32] or low wind speeds [5, 11, 12, 14, 21, 22, 33]. Numerous studies only analyze a subset of observations associated with near thermally neutral conditions, i.e. weakly stable, neutral, or weakly unstable conditions, while they do not consider very stable or unstable conditions [12, 14, 16, 17, 22, 28]. Only a few studies have reported less commonly used turbulence statistics, such as integral timescales, integral lengthscales, spectral wavelengths, two-point correlations, and high order statistics (e.g. skewness and kurtosis). Such statistics are informative for describing turbulence structures in the urban atmosphere [6, 7, 16, 37, 44, 45]. Systematic scaling studies of turbulence parameters, such as variances and fluxes, have been limited, although such analyses are very informative in urban canopy model parameterization [7, 22, 40, 45]. An overall assessment of the literature indicates that many urban microclimate field studies encourage more field campaigns to investigate the urban microclimate at greater detail, under diverse physical conditions, and with alternative statistical descriptions of turbulence [11, 32, 33, 49].

2 Objectives

The present study will attempt to understand and quantify flow and temperature dynamics in an urban canyon under a comprehensive set of wind directions, wind speeds, and thermal stability conditions. This approach will be complementary to other studies

where only limited conditions in wind directions, wind speeds, and thermal stabilities have been considered. This study will also perform a rigorous scaling analysis to find significant statistical correlations among various mean and turbulence statistics describing the flow and temperature dynamics in the rural and urban sites.

3 Methodology

The urban microclimate campaign occurred from 13th to 25th of August 2017 in Guelph, Ontario, Canada. This time window corresponds to hot summer conditions, which is of concern and interest in many geographical areas under urban heat island (UHI) stress.

3.1 Site logistics

Figure 1 shows the logistics of the urban and rural sites utilized in this urban climate study. The urban canyon site, the Reek Walk, is located at the University of Guelph's main campus, Guelph, Ontario, Canada, at 43.5323°N and 80.2253°W. The rural site, the Guelph Turfgrass Institute, is located at 43.5473°N and 80.2149°W, Northeast of the campus. The urban canyon axis is oriented at − 45° with respect to the North. The cross-canyon direction is x with wind velocity component U, and the along-canyon direction is y with wind velocity component V. The vertical direction is z with the wind velocity component W. Two test areas are designated in the urban site: one inside the Reek Walk canyon and another on the roof of the Rozhanski Hall building (see Fig. 1a). The average height of surrounding buildings is $H_{avg} = 12.2$ m, and the canyon height and length are $H = 13$ m and $L = 55$ m, respectively, with unit canyon aspect ratio (ratio of canyon width to canyon height). The distance between the urban and rural sites is 2.13 km and the surface roughness lengthscale of the canyon is $h = 0.1$ m [13]. As can be seen in Fig. 1a, half of the street canyon is covered with asphalt and the other half is covered with grass. Albedos of gravel (roof), red brick (canyon walls), asphalt (street), and dry grass (street) are 0.3, 0.2–0.3, 0.08–0.18 and 0.3, respectively [13, 42]. The Reek Walk was cordoned off during the study.

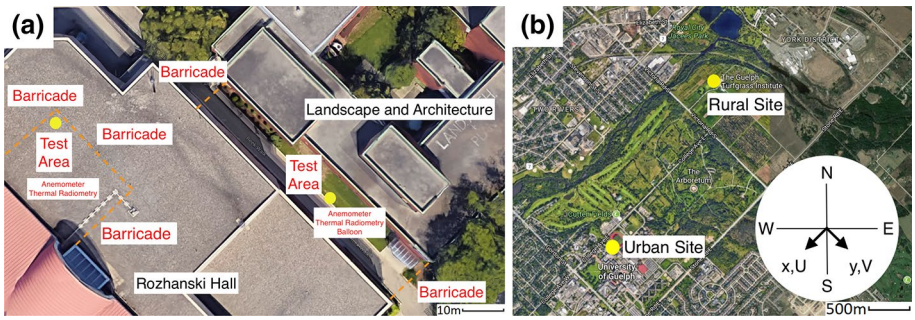

Fig. 1 Top view of **a** high resolution urban site at the University of Guelph and **b** low resolution urban site plus rural site (Guelph Turfgrass Institute); annotations are superimposed on Google maps

3.2 Instrumentation

The rural site climate data is accessed via Environment and Climate Change Canada's online portal, available at http://climate.weather.gc.ca/historical_data/search_historic_data_e.html. The Guelph Turfgrass Institute station is identified with World Meteorological Organization (WMO) identification number 71833. This data is accessible with an hourly time resolution. Temperature data is collected at 2 m above grade while wind data is collected at 10 m above grade.

Two fixed weather stations were installed in the urban site, one in the middle (and centre with respect to the x direction) of the Reek Walk and another on the roof of Rozhanski Hall. The weather stations measured meteorological conditions 2 m above surface level, either at the street or roof levels. Two R. M. Young 81000 sonic anemometers were used in the weather stations. They sampled air velocities in the x, y, and z directions as well as the sonic air temperature at a frequency of 4 Hz during the entire campaign using two Campbell Scientific CR1000 data loggers. The anemometers' measurement resolutions were 0.01 m s^{-1} for wind speed and 0.01 K for sonic temperature. The upper limit for the sampling frequency was determined by the data loggers and the volume of data desired for the analysis. Additionally, the anemometer data was also logged at 32 Hz for short periods (twelve hours) during intensive observation periods using two laptops to compare with the 4 Hz-sampled data. Numerous studies report sonic anemometer sampling at 10 Hz [5, 11, 21, 22, 32, 33, 38, 49], 20 Hz [6, 7, 12, 38], or > 20 Hz [12, 16, 17, 28, 33, 40] for field campaigns focused on turbulence measurements. The sonic anemometer data were time averaged for intervals of 30 min to compute turbulent fluctuations at the microscale. Various periods of averaging have been used in the literature while sampling high frequency data such as 15 min [5], 30 min [6, 7, 22], and 1 h [6]. A Campbell Scientific HMP60 temperature and relative humidity probe was used at the street weather station to collect minute-averaged temperature and relative humidity data. A Pace Scientific SRS-100 solar radiation sensor was used at the roof weather station to collect minute-averaged downwelling solar radiation. The resolution for this sensor was 1 W m^{-2}.

A custom-designed balloon sensing platform was developed to obtain vertical profiles of temperature and relative humidity (RH) at the urban site during selected times. The system was dubbed the Tethered And Navigated Air Blimp (TANAB). The balloon was filled with helium to a diameter of approximately 1.5 m to generate a buoyancy force sufficient to levitate a gondola housing the sensor suite while a human operator controlled it from the ground using a tether. It measured temperature using a type T thermocouple connected to an Adafruit Universal Thermocouple Amplifier MAX31856 Breakout board. The thermocouple had a resolution of 0.01 K. TANAB measured RH using an Adafruit DHT11 sensor. The accuracy of this sensor was 5%, while the precision was 1%. TANAB also measured its position in three dimensions using a Pozyx position sensor. This sensor relied on ultra wideband (UWB) technology to give position within 0.1 m while the airborne circuit communicated with fixed antennas on the walls of the urban canyon. The sensors were connected to an Arduino Mega board and data was written onboard on an Adafruit MicroSD card. TANAB sampled the environment at a frequency of 0.33 Hz.

Thermal imaging of the urban surfaces was performed using a FLIR E4 thermal camera. During intensive observation periods, this camera was pointed at multiple locations including the roof (one location), canyon walls (six locations), asphalt (two locations),

and grass (two locations). During these periods three measurements at each location were made at 1-h time intervals. The resolution of the camera was 0.1 K. Images collected were processes statistically by calculating mean temperatures and the standard deviations at every location for every hour.

Essential to the measurements was the elimination of any bias among different temperature sensors. Temperature bias correction was performed by running every sensor against the HMP60 sensor in laboratory conditions, and calculating the biases and eliminating them during data analysis. The sonic anemometers were also re-calibrated by the manufacturer prior to the field campaign.

3.3 Calculations of turbulence statistics

In this study Reynolds decomposition is used for analysis, e.g. $U = \overline{U} + u$, where U is the cross-canyon velocity component. Due to the lack of the availability of the ensemble average of a variable, e.g. $\langle U \rangle$, the 30-min time average of the variable, e.g. $\overline{U}$, is used instead. Likewise, variances are shown by $\overline{u^2}$, $\overline{v^2}$, $\overline{w^2}$, and $\overline{t^2}$, and the Reynolds stresses and turbulence fluxes are shown by $\overline{uv}$, $\overline{uw}$, $\overline{vw}$, $\overline{ut}$, $\overline{vt}$, and $\overline{wt}$.

The integral timescales are calculated for each 30-min interval using the autocorrelation function $\mathcal{R}$. For example, $\mathcal{R}_{UU} = \overline{u(\tau)u(\tau + s)}$, where s is time shift. For example for U component of velocity the integral timescale is

$$\mathcal{T}_{UU} = \frac{1}{\overline{u^2}} \int_0^\infty \mathcal{R}_{UU}(s) ds. \tag{1}$$

In practice, however, these integrals are only integrated to a large enough time shift s, usually < 5 min in urban microclimate measurements, so far as the autocorrelation does not become negative. This has been justified by the fact that larger eddies, thermal structures, and diurnal variations in the atmosphere, are present that result in negative autocorrelations over long time shifts [2]. Such slow and large scale events are characteristic of weather [47] and are not considered within the scales of turbulence in urban canopy microclimate modelling.

Integral lengthscales in this study are calculated using Taylor's hypothesis [46], given the fact that the observed turbulence intensities are smaller than 0.5 [48]. For example the following relationship relates the integral timescale to the integral lengthscale:

$$\mathcal{L}_{UU} = \overline{U} \times \mathcal{T}_{UU}. \tag{2}$$

Although the Taylor's hypothesis has been proclaimed as limited in urban flows since turbulence intensities can be > 0.5 [32, 33, 37], some studies have used it to estimate integral lengthscales, at least in regions of the flow where turbulence intensity was expected to be < 0.5 [44, 45]. Other studies have recommended using limited two-point correlation observations to estimate the integral lengthscales [37]. Two-point autocorrelation functions are calculated for all pairs of variables. For example for U and V it is

$$\mathcal{R}_{UV}(\mathbf{r}, \mathbf{x}) = \overline{u(\mathbf{x} + \mathbf{r}, \tau) v(\mathbf{x}, \tau)}, \tag{3}$$

where $\mathbf{x}$ is the position vector for the location of the street weather station and $\mathbf{r}$ is the vector pointing from the street weather station to the roof weather station. The structure functions are calculated for all pairs of variables. For example for U and V it is

$$\mathcal{D}_{UV}(\mathbf{r}, \mathbf{x}) = \overline{[U(\mathbf{x} + \mathbf{r}, \tau) - U(\mathbf{x}, t)][V(\mathbf{x} + \mathbf{r}, \tau) - V(\mathbf{x}, \tau)]}. \tag{4}$$

In each 30-min time interval, the time series of high frequency measurements were detrended before turbulence statistics were calculated. That is, a linear trend was first fitted to each 30-min time interval and then removed from the time series. This was to ensure that slow background variations in wind and temperature measurements, that signify weather variation, would not influence the turbulence statistics calculations [47]. Except for mean quantities and the structure functions, all other turbulence statistics are calculated after deterending the time series.

4 Results and discussion

4.1 Time series for meteorological conditions

Hourly time series plots of wind speed and wind direction are shown in Fig. 2. The wind speed at roof level is reduced compared to the rural site and the wind direction is also modified compared to the rural site. This is due to the fact that the urban roughness affects the flow field in and above the canopy so it is expected that the wind speed above the roof is affected by a combination of morphological and meteorological factors. Wind speeds at street level are significantly lower than roof level due to building drag [25]. Wind directions at street level generally either follow the roof-level wind direction, indicative of a predominantly channeling flow, or oppose the wind direction at roof level, indicative of the formation of a strong vortex flow in the canyon with an axis aligned with the canyon axis.

Figure 3 shows hourly time series plots of temperatures (or temperature differences) and the bulk Richardson number (to be defined in Sect. 4.2). The mean value of walls and street surface temperatures is denoted by canyon surface temperature, and the mean value of all surface temperatures including the roof, walls, and street is denoted by urban surface temperature. In addition to atmospheric temperatures, the urban surface temperatures are also

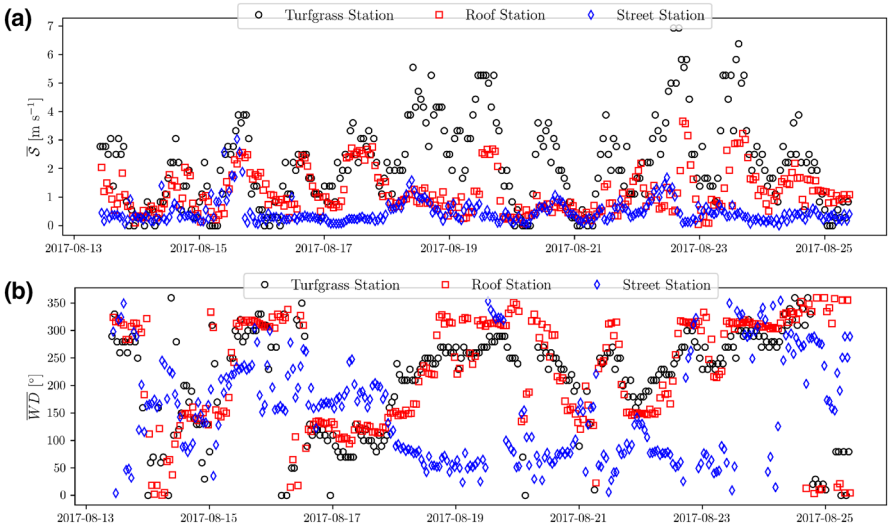

Fig. 2 Hourly time series starting from 1100 local solar time (LST) on 13 August 2017: **a** time-averaged wind speed ($S = (\overline{U}^2 + \overline{V}^2)^{1/2}$) and **b** time-averaged wind direction

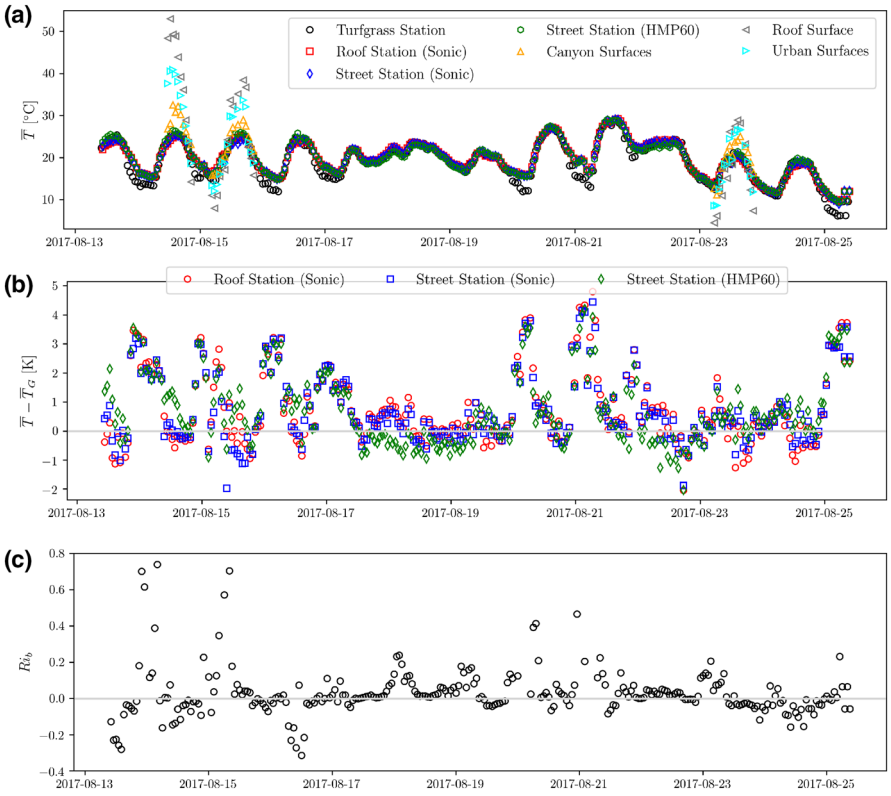

Fig. 3 Hourly time series for: **a** atmospheric and urban surface temperatures, **b** atmospheric temperature ($\overline{T}$) minus rural temperature ($\overline{T}_G$), and **c** bulk Richardson number (Ri_b)

measured for selected periods. It can be observed that the urban surface temperatures oscillate with a greater amplitude compared to the urban atmospheric temperatures. That is, hotter temperatures during the days and colder temperatures during the nights are observed for urban surfaces. As also commonly found in the literature, the temperature oscillations for the roof surface were greater than that of the canyon surfaces, when low albedo roofs were monitored [23]. The mean urban heat island (UHI) intensity, measured as the difference between urban street level and rural atmospheric temperatures, is measured as 0.7 K with a standard deviation of 1.2 K for the entire dataset. The magnitude of UHI is reduced during cloudy conditions for a period from 17 August 2017 to 20 August 2017. The UHI quantified in this study for Guelph is significantly lower than observations in metropolitan areas. For instance Barlow et al. [6] report an average UHI of 4 K by night and 1.5 K by day for London (U.K.) in September and October of 2011. As reported commonly in the literature, the UHI intensity was observed to peak during the nights [4]. The difference between the roof-level atmospheric temperature and the street-level atmospheric temperature indicates periods of thermal stability during the nights and periods of thermal instability during the days as indicated by the bulk Richardson number.

Figure 4 shows the canyon surface temperatures and temperature differences in different locations. The top of NE and SW walls experience a temperature difference by up to 10 K as

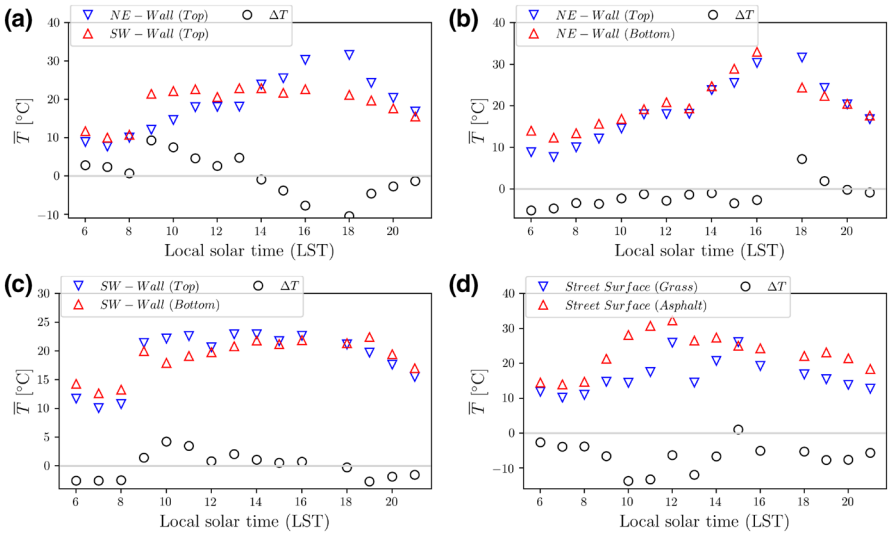

Fig. 4 Hourly temperature and temperature difference between different locations at canyon walls and street for: **a** top of NE and SW walls, **b** top and bottom of NE wall, **c** top and bottom of SW wall, and **d** between grass and asphalt; top location refers to the highest 4.33 m and bottom location refers to the lowest 4.33 m on the canyon walls

a function of diurnal time. The top and bottom of each wall also experience a temperature difference up to 5 K. These observations are in agreement with those performed by Offerle et al. [34] and Santamouris et al. [43]. The difference between grass and asphalt surface temperatures at street level during the day is as much as 10 K, with the grass being colder than asphalt.

Not shown is the time series of the hourly-average relative humidity. It was observed that the rural site was more humid than the urban site at all times, with the difference being the highest up to 15% during the nights.

4.2 Building Reynolds mumber and bulk Richardson number

Inertial and thermal stability conditions at the urban site are given by the building Reynolds number and bulk Richardson number, respectively. The building Reynolds number Re_H is calculated using horizontal wind speed, either at the rural site or at the building roof level, and is given by

$$Re_H = \frac{(\overline{U}^2 + \overline{V}^2)^{1/2} H}{\nu} = \frac{\overline{S} H}{\nu}, \tag{5}$$

where H is the building height, $\overline{U}$ and $\overline{V}$ are time-averaged horizontal wind velocities in the x and y directions, $\overline{S}$ is the time-averaged horizontal wind speed, and ν is air's kinematic viscosity. The bulk Richardson number Ri_b is given by

$$Ri_b = \frac{gH}{(\overline{U}_R - \overline{U}_S)^2 + (\overline{V}_R - \overline{V}_S)^2} \frac{\overline{T}_R - \overline{T}_S}{\overline{T}_A}, \tag{6}$$

where g is gravitational acceleration and $\overline{T}$ is time-averaged absolute temperature. Subscripts R and S signify roof-level and street-level measurements by the sonic anemometers. The reference temperature $\overline{T}_A$ is given by the average temperature of $\overline{T}_R$ and $\overline{T}_S$. Ideally, $\overline{T}_R$ and $\overline{T}_S$ should be measured adjacent to roof and street levels. However, due to the limited number of sonic anemometers in this study, they have been measured 2 m above each surface. Given the fact the the bulk Richardson number is calculated over a short vertical distance in the urban roughness sublayer, we do not restrict the bulk Richardson number to a critical value to indicate the onset of thermal stability. Rather, it is considered that all positive values indicate the thermally stable condition, all negative values indicated the thermally unstable condition, and near zero values indicate the thermally neutral condition. This is in contrast to numerous studies in the literature that analyzed the bulk Richardson number over a substantial depth of the boundary layer and defined a critical bulk Richardson number to indicate the onset of thermal stability. Many such critical Richardson numbers are reviewed by Ohya [35].

Figure 5 shows the diurnal variations of Re_H and Ri_b. Inertial effects dominate during the day and peak in the mid afternoons. The thermal stability of the urban atmosphere oscillates between stable to unstable conditions from early mornings to mid afternoons. A period of neutrally stable conditions is observed in the early afternoon and evening periods.

4.3 Analysis of flow and temperature dynamics

Since roof-level wind direction relative to the canyon axis has been reported to significantly influence flow and temperature dynamics in the urban canyon [5, 11, 21, 22, 49], the data is classified according to roof-level wind angle. Eight wind angles are considered that each cover 45°: North (N), Northeast (NE), East (E), Southeast (SE), South (S), Southwest (SW), West (W), and Northwest (NW). Out of these, two wind angles are along the canyon axis (NW, SE), two wind angles are perpendicular to the canyon axis (NE, SW), and four wind angles are oblique (N, E, S, W) (see Fig. 1). Turbulence statistics, including means, variances, covariances, etc. are classified into 24 diurnal times, building Reynolds numbers, and bulk Richardson numbers, for each wind angle. These wind angles, diurnal times, building Reynolds numbers, and bulk Richardson numbers provided a statistic for most combinations. All data from multiple days has been used for the data classification. To avoid clutter in the figures, only the statistical median for each wind angle is shown. However, in Sect. 4.9 where a scaling analysis is performed, the entire dataset is considered.

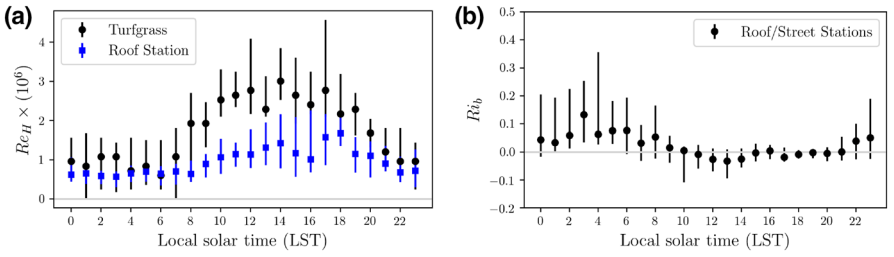

Fig. 5 Inertial and thermal stability conditions in the urban site over multiple days: **a** building Reynolds number (Re_H) and **b** bulk Richardson number (Ri_b); the markers indicate medians and the ranges represent 25th and 75th percentiles of the data distributions

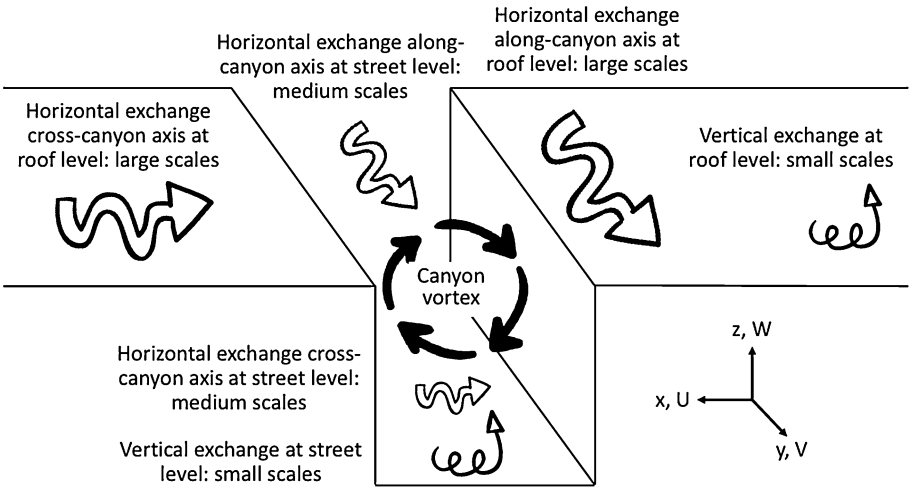

Fig. 6 Schematic showing the main canyon vortex and various exchange components in the horizontal and vertical directions; the size of the arrows indicates the integral scale of the exchange process

It is important to consider Fig. 6 before reading the following subsections. This figure shows that various exchange processes for momentum and heat can be considered in the horizontal and vertical directions. The horizontal motions consist of along-canyon and cross-canyon axes. Furthermore, these exchanges can be considered either at street-level or roof-level weather stations. The scale of the exchange process refers to the integral timescale and integral lengthscale to be discussed in Sect. 4.6.

4.4 Mean flow and temperature

Figure 7 shows the hourly mean wind speed, velocity components, and temperatures at roof-level and street-level weather stations. The plots for $\overline{U}$ and $\overline{V}$ indicate that the data has been correctly classified according to wind angle. Particularly, the plots of $\overline{U}$ for cross and oblique-flow conditions show that the sign of $\overline{U}$ is reversed from roof to street-level measurements, which is indicative of the presence of vortex flow inside the canyon. Plots of the vertical component of the wind $\overline{W}$ indicate that for many wind directions the mean vertical motion of air is up to ± 0.1 m s^{-1}. This can be attributed to the three-dimensionality of the urban environment and variety of building heights at the vicinity of the site. The plots for temperature $\overline{T}$ show the diurnal cooling and heating of the air although the temperature curves shift up and down due to temperature variations over multiple days during the measurement campaign, as shown in Fig. 3a. The wind blowing from the South passes through more urbanized areas, where the effect of UHI is significant. Thus, wind blowing from the South is always warmer.

4.5 Turbulence statistics: variances and covariances

Figure 8 shows variances (within 30-min time intervals) of velocities and temperature as measured by both the roof-level and street-level weather stations. All variances exhibit a peak during mid day or thermally unstable conditions. The variances also exhibit greater

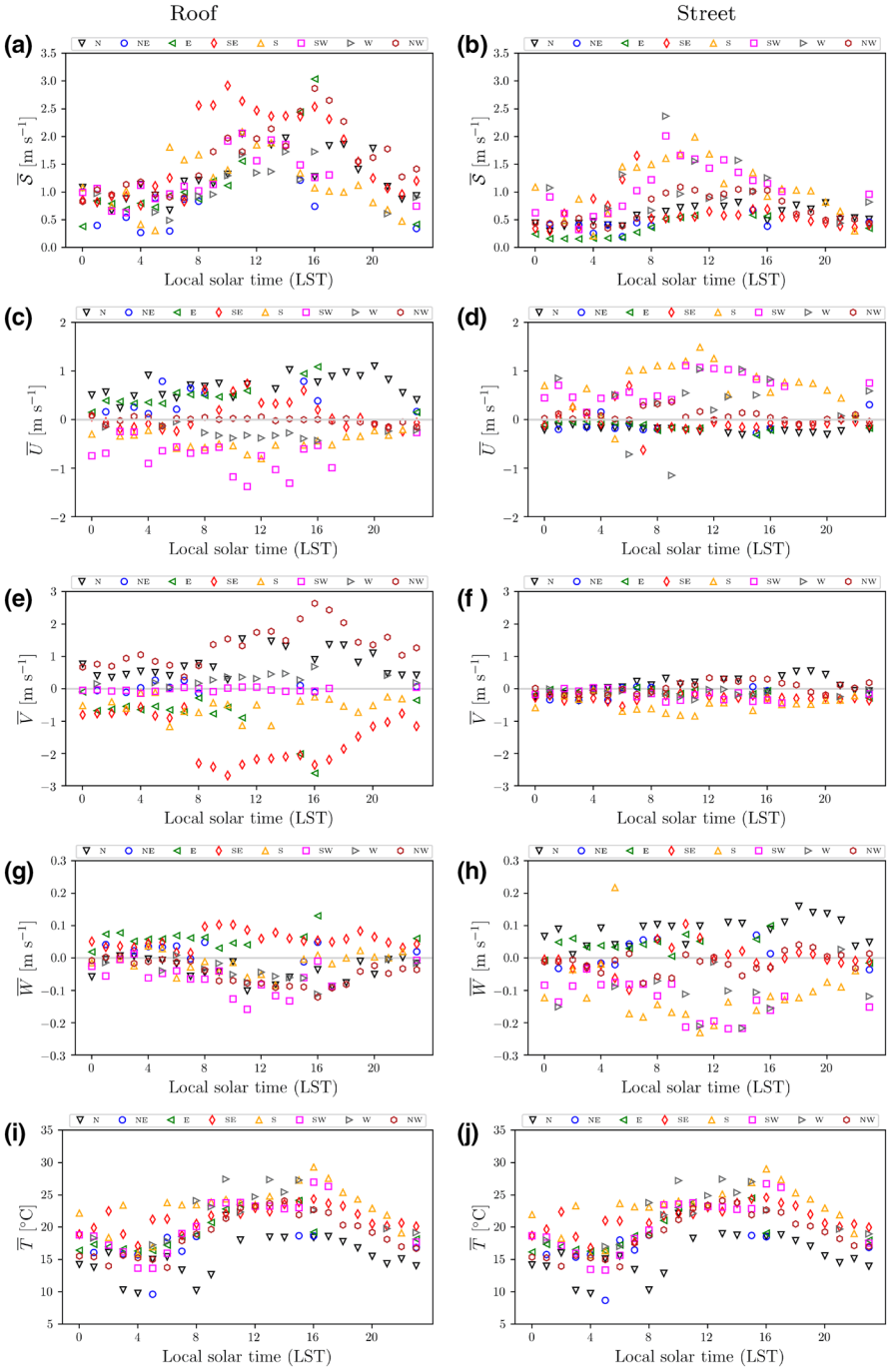

Fig. 7 Hourly mean wind speed $\overline{S}$ (**a**, **b**), velocities $\overline{U}$ (**c**, **d**), $\overline{V}$ (**e**, **f**), $\overline{W}$ (**g**, **h**), and temperature $\overline{T}$ (**i**, **j**), classified based on the roof wind angle and diurnal time for roof station shown on the left panel (**a**, **c**, **e**, **g**, **i**) and street station shown on the right panel (**b**, **d**, **f**, **h**, **j**)

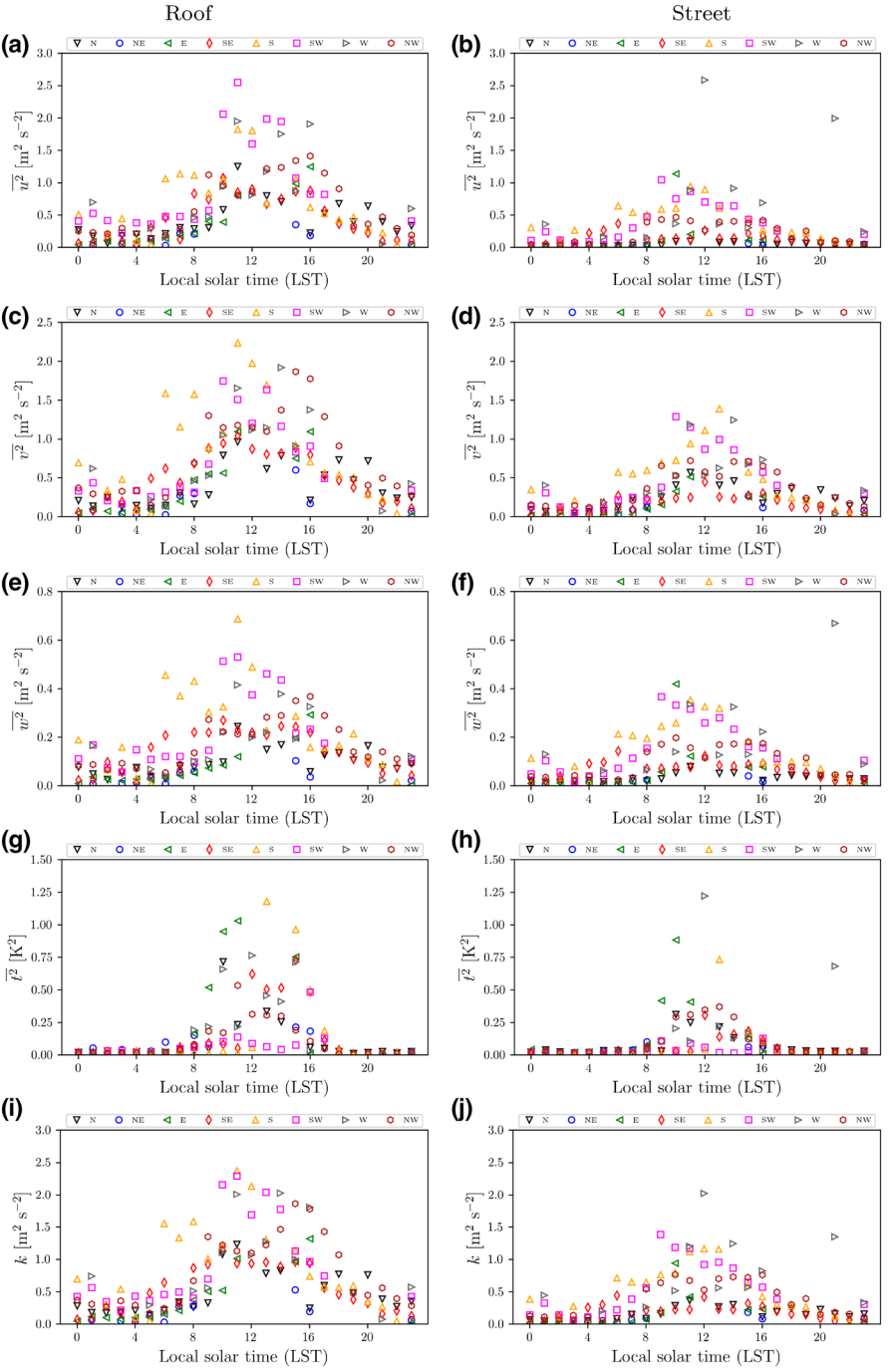

Fig. 8 Hourly variances of velocities $\overline{u^2}$ (**a**, **b**), $\overline{v^2}$ (**c**, **d**), $\overline{w^2}$ (**e**, **f**), temperature $\overline{t^2}$ (**g**, **h**), and turbulence kinetic energy (TKE) k (**i**, **j**), classified based on the roof wind angle and diurnal time for roof station shown on the left panel (**a**, **c**, **e**, **g**, **i**) and street station shown on the right panel (**b**, **d**, **f**, **h**, **j**)

magnitudes for certain wind directions. Velocity variances and the turbulence kinetic energy (TKE) k show higher magnitudes for S, SW, W, and NW wind directions at both weather stations. The temperature variance shows higher magnitudes for E, SE, S, W, and NW wind directions. It is speculated that heterogeneity in urban morphology and surface temperatures may be responsible for these observations. A lower magnitude is observed in the velocity and temperature variances at the street level compared to the roof level. A higher temperature variance at the roof level can be explained by the fact that it is well known that the roof surface temperature exhibits a greater temperature difference with the atmosphere compared to canyon surfaces [23], hence influencing $\overline{t^2}$ more significantly.

Figure 9 shows the Reynolds Stresses, or equivalently turbulence kinematic momentum fluxes. The horizontal flux $\overline{uv}$ is consistently positive or negative for certain wind angles (e.g. S, W, NW), which suggests that horizontal flux gradients may be present in the wind field. This is a micrometeorological feature of the site although such horizontal flux gradients were not measured given the limited number of anemometers used at the site. The vertical components of the flux, i.e. $\overline{uw}$ and $\overline{vw}$ can be examined to observe which way momentum is transported, upward or downward, for a given wind angle. For $\overline{uw}$, wind angles with a significant U component shall be analyzed. At roof level, when U is negative

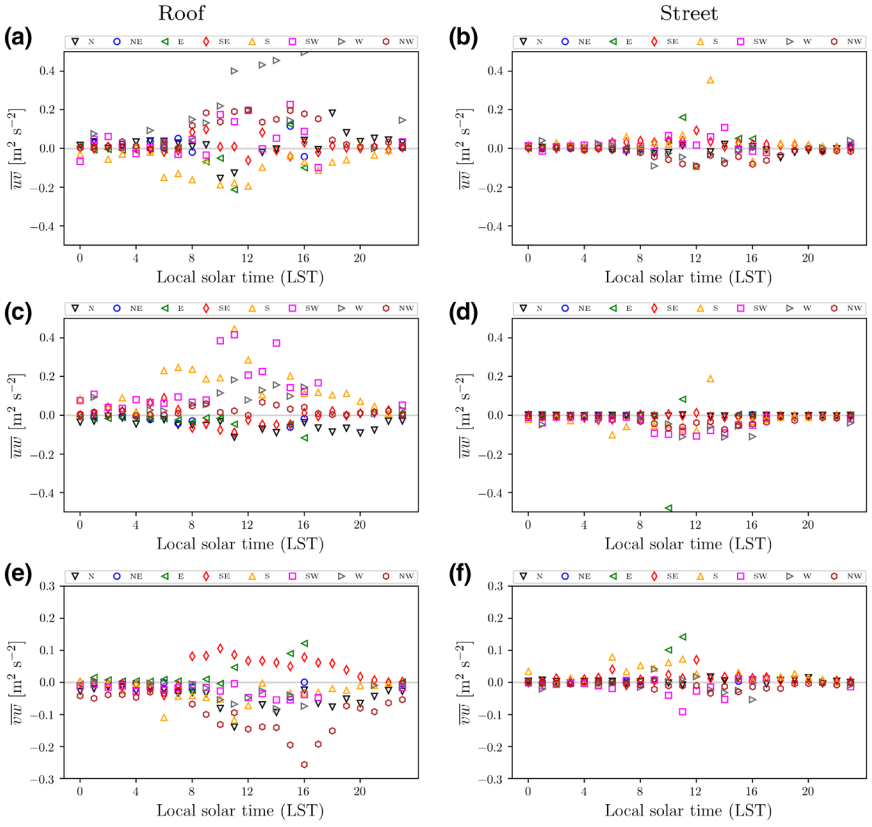

Fig. 9 Hourly Reynolds stresses $\overline{uv}$ (**a**, **b**), $\overline{uw}$ (**c**, **d**), and $\overline{vw}$ (**e**, **f**), classified based on the roof wind angle and diurnal time for roof station shown on the left panel (**a**, **c**, **e**) and street station shown on the right panel (**b**, **d**, **f**)

(S, SW, W), $\overline{uw}$ is positive, and when U is positive (N, NE, E), $\overline{uw}$ is negative. This consistently confirms that the U component of the momentum is transported downward at roof level due to the $\overline{uw}$ flux. A similar argument can be made for transport of the U component of the momentum downward at street level. In this case, although the signs of $\overline{uw}$ are reversed (see E, S, SW legends), the presence of the canyon vortex indicates a downward transport of momentum. For $\overline{vw}$, wind angles with a significant V component shall be analyzed. At roof level, when V is negative (E, SE), $\overline{vw}$ is positive, and when V is positive (W, NW, N), $\overline{vw}$ is negative. This consistently confirms that the V component of the momentum is transported downward at roof level due to the $\overline{vw}$ flux. A similar argument can be made for transport of the V component of the momentum downward at street level. However, in this case a switching of the sign for the flux is not observed since no primary vortex with an axis normal to that of the canyon is expected in the canyon.

Figure 10 shows the turbulence kinematic heat fluxes. There is clearly a diurnal dependence on the magnitude of the heat flux. Similar to the analysis of horizontal Reynolds stresses, we shall confirm the presence of horizontal heat fluxes by identifying opposing signs of the flux in a direction associated with opposing wind angles along that direction.

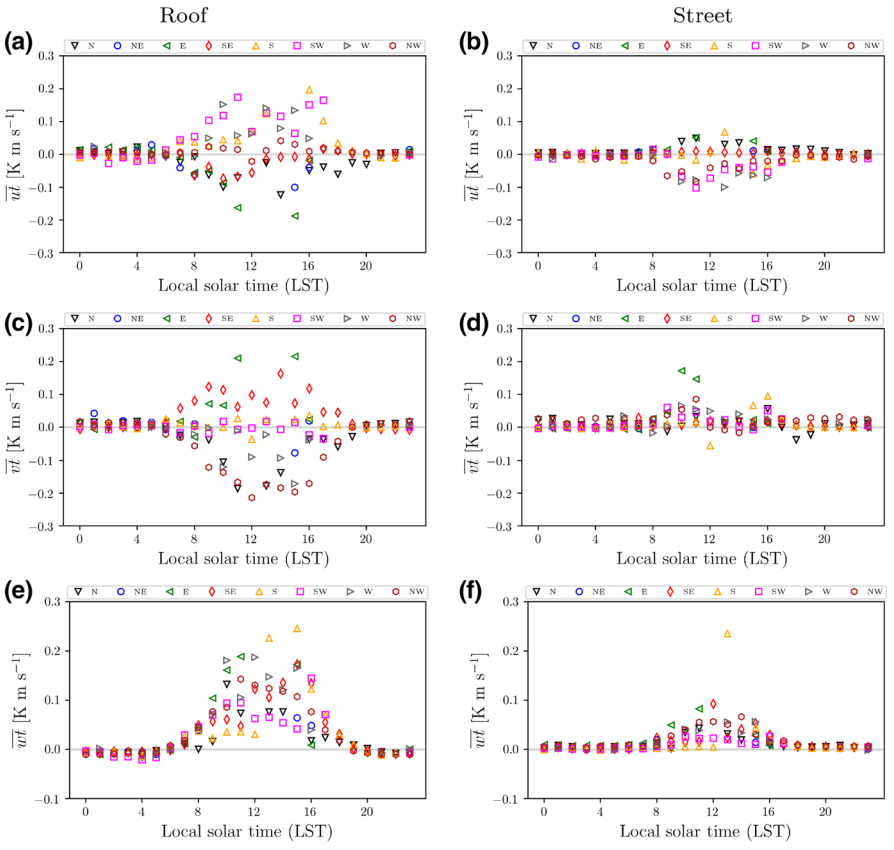

Fig. 10 Hourly turbulence heat fluxes $\overline{ut}$ (**a**, **b**), $\overline{vt}$ (**c**, **d**), and $\overline{wt}$ (**e**, **f**), classified based on the roof wind angle and diurnal time for roof station shown on the left panel (**a**, **c**, **e**) and street station shown on the right panel (**b**, **d**, **f**)

For roof-level flux $\overline{ut}$, we observe positive values associated with wind angles S, SW, and W, while we observe negative values for wind angles N, NE, and E. This clearly shows there is turbulence heat flux in the x direction. For the same direction at street level, the signs for the horizontal flux reverse, again due to the presence of the main canyon vortex. For the roof-level flux $\overline{vt}$ we observe positive values associated with wind angles E and SE, while we observe negative values for wind angles W, NW, and N. This clearly shows there is turbulence heat flux in the y direction. In this direction, the signs for flux do not switch at street level since no primary vortex with an axis normal to that of the canyon is expected in the canyon. The vertical heat flux $\overline{wt}$ is slightly negative during thermally stable conditions, while it is significantly positive during the thermally unstable conditions. This is contrary to some observations reporting no negative vertical heat flux whatsoever for other mid-latitude locations [38]. The magnitude of the vertical heat flux is greater at roof level compared to the street level. Again, this can be justified by the well-known fact that wind speeds and surface-atmosphere temperature differences are greater at roof level in most locations [23].

Figure 11 shows the variations of temperature variance and TKE versus the building Reynolds number. Temperature variance at roof level exhibits a peak corresponding to moderate wind speeds ($0.9 < \overline{S} < 1.7$) indicating that either low or high wind conditions suppress turbulent fluctuations of temperature. This phenomenon is not observed near street level, possibly due to lower wind speeds. TKE shows an increasing trend as a function of building Reynolds number for both roof-level and street-level weather stations. A threshold wind speed of 0.9 m s^{-1} can be observed for the onset of temperature variance and TKE. Other studies also found a threshold for wind speed to establish correlation between the above-roof and street-level winds [11, 43].

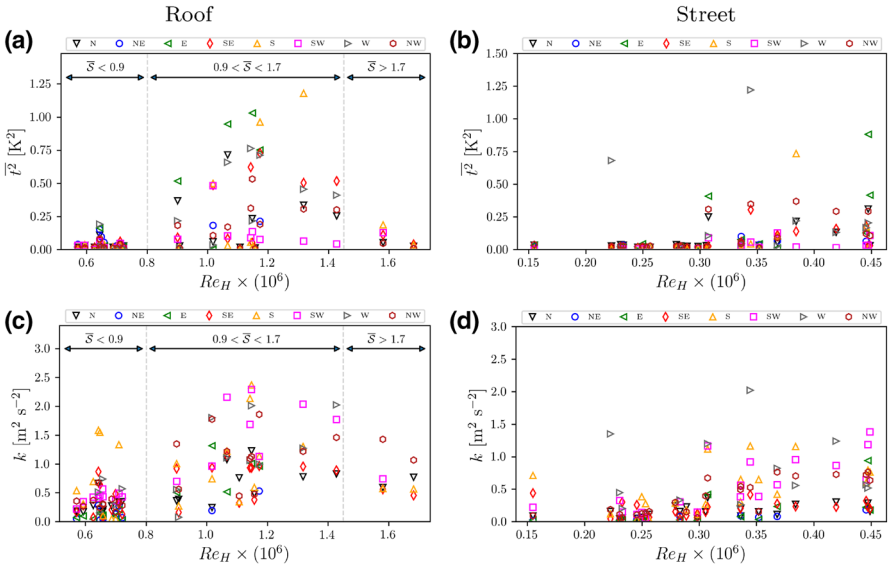

Fig. 11 Hourly variance of temperature $\overline{t^2}$ (**a**, **b**), and turbulence kinetic energy (TKE) k (**c**, **d**), classified based on the roof wind angle and the building Reynolds number Re_H for roof station shown on the left panel (**a**, **c**) and street station shown on the right panel (**b**, **d**)

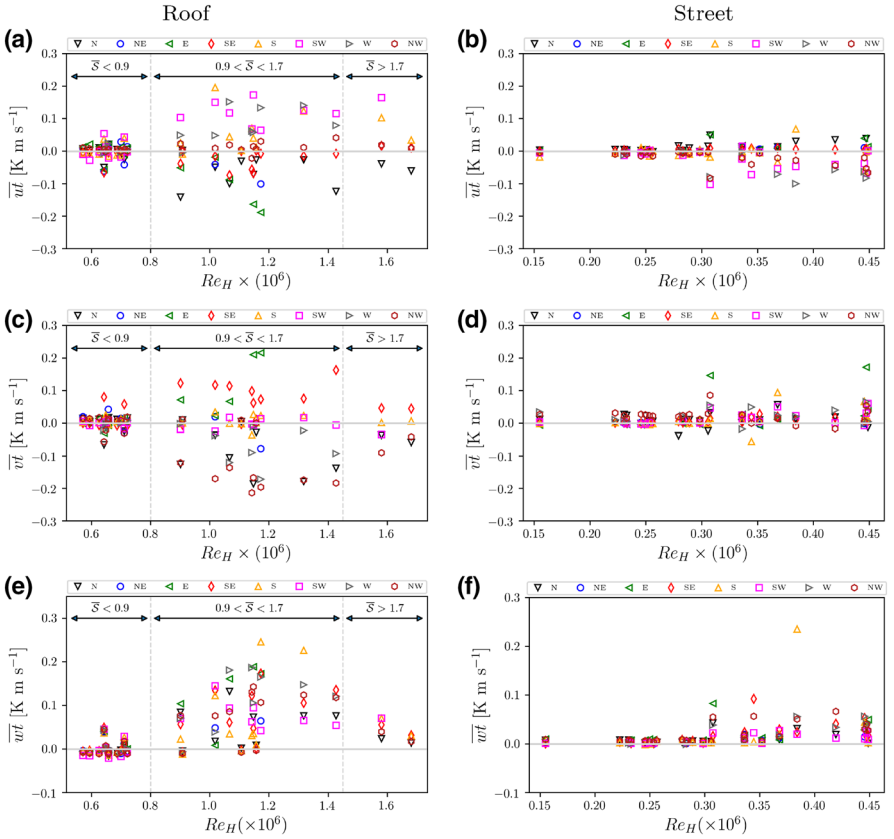

Fig. 12 Hourly turbulence heat fluxes $\overline{ut}$ (**a**, **b**), $\overline{vt}$ (**c**, **d**), and $\overline{wt}$ (**e**, **f**), classified based on the roof wind angle and the building Reynolds number Re_H for roof station shown on the left panel (**a**, **c**, **e**) and street station shown on the right panel (**b**, **d**, **f**)

Figure 12 shows the variations of turbulence heat fluxes as a function of the building Reynolds number. A threshold wind speed of 0.9 m s^{-1} can be observed for the occurrence of significant heat fluxes. In agreement with Fig. 10, horizontal fluxes of heat can be either positive or negative, i.e. directional, depending on the wind direction, but the vertical heat flux is positive regardless of the wind direction, provided that the wind speed is above the 0.9 m s^{-1} threshold.

Figure 13 shows the variations of temperature variance and TKE versus the bulk Richardson number. With increasing thermal stability the variance and TKE decline. The decline is gradual and there is no evidence whether a critical bulk Richardson number is required to define thermal stability when calculating the bulk Richardson number within the lower portion of the urban roughness sublayer.

Figure 14 shows the variations of turbulence heat fluxes as a function of the bulk Richardson number. With increasing thermal stability the heat fluxes decline. Again, the decline is gradual. In agreement with Fig. 10, horizontal fluxes of heat can be either positive or negative, i.e. directional, depending on the wind direction, but the vertical

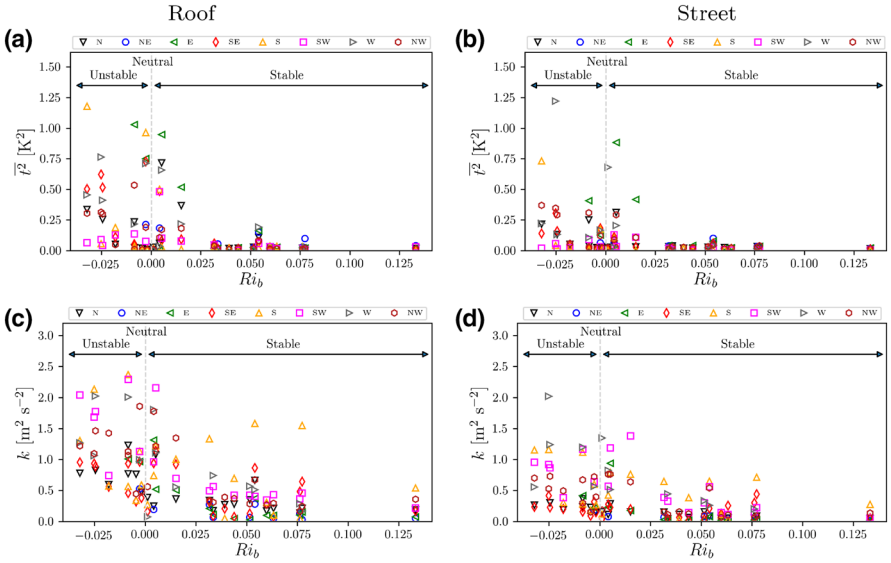

Fig. 13 Hourly variance of temperature $\overline{t^2}$ (**a**, **b**), and turbulence kinetic energy (TKE) k (**c**, **d**), classified based on the roof wind angle and the bulk Richardson number Ri_b for roof station shown on the left panel (**a**, **c**) and street station shown on the right panel (**b**, **d**)

heat flux is positive regardless of the wind direction, provided that the urban canopy air is near neutral or thermally unstable.

4.6 Turbulence statistics: integral scales

Table 1 shows the integral timescales calculated for each mean velocity component and mean temperature. The integral timescales do not exhibit a diurnal variation. However, the integral timescales $\mathcal{T}_{UU}$, $\mathcal{T}_{VV}$, and $\mathcal{T}_{TT}$ are by a factor of 5–10 > $\mathcal{T}_{WW}$. This suggests that turbulent eddies and thermal structures in the horizontal direction are longer-lived than those in the vertical direction.

Table 2 shows the integral lengthscales. The integral lengthscales do not exhibit a significant diurnal variation at roof or street-level stations either. $\mathcal{L}_{UU}$ and $\mathcal{L}_{VV}$ at street level are a factor of two to three lower than those at roof level. Integral lengthscales $\mathcal{L}_{WW}$ are more than one order of magnitude smaller than $\mathcal{L}_{UU}$ and $\mathcal{L}_{VV}$. $\mathcal{L}_{WW}$ at the street-level station is greater than that at the roof-level station by a factor of five. This can be explained by higher mean vertical velocity observations at the street-level station as shown in Fig. 7g, h.

4.7 Turbulence statistics: two-point correlations

Although the application of the Taylor hypothesis is questionable within the urban roughness sublayer (RSL), the integral lengthscales obtained in Sect. 4.6 can be put in context by studying the two-point autocorrelation functions presented here. For example, the integral lengthscale corresponding to U velocities is defined by

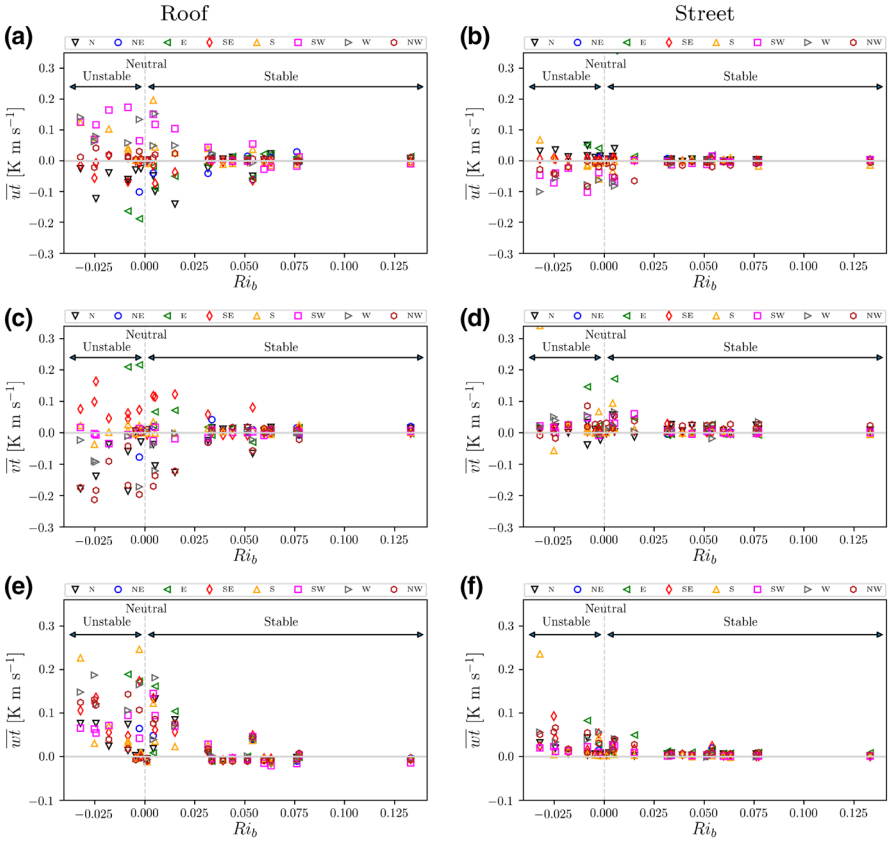

Fig. 14 Hourly turbulence heat fluxes $\overline{ut}$ (**a**, **b**), $\overline{vt}$ (**c**, **d**), and $\overline{wt}$ (**e**, **f**), classified based on the roof wind angle and the bulk Richardson number Ri_b for roof station shown on the left panel (**a**, **c**, **e**) and street station shown on the right panel (**b**, **d**, **f**)

Table 1 Statistical percentiles of integral timescale

Timescale	Location					
	Roof			Street		
	Lwr.	*Med.*	*Upr.*	*Lwr.*	*Med.*	*Upr.*
$\mathcal{T}_{UU}$ (s)	5.41	9.11	15.85	5.75	9.39	14.94
$\mathcal{T}_{VV}$ (s)	7.80	12.45	19.60	9.55	14.73	23.21
$\mathcal{T}_{WW}$ (s)	1.20	1.88	3.03	1.80	3.21	5.36
$\mathcal{T}_{TT}$ (s)	7.07	11.88	19.64	10.29	16.98	26.09

Upr. upper quartile, *Med.* median, *Lwr.* lower quartile

$$\mathcal{L}_{UU}(\mathbf{x}) = \frac{1}{\mathcal{R}_{UU}(0,\mathbf{x})}\int_0^\infty \mathcal{R}_{UU}(r\mathbf{e},\mathbf{x})dr, \tag{7}$$

Table 2 Statistical percentiles of integral lengthscale

Lengthscale	Location					
	Roof			Street		
	Lwr.	*Med.*	*Upr.*	*Lwr.*	*Med.*	*Upr.*
$\mathcal{L}_{UU}$ (m)	0.67	1.69	5.27	0.72	1.76	4.96
$\mathcal{L}_{VV}$ (m)	4.94	10.50	20.09	1.39	2.88	5.34
$\mathcal{L}_{WW}$ (m)	0.04	0.08	0.15	0.07	0.19	0.37

Upr. upper quartile, *Med.* median, *Lwr.* lower quartile

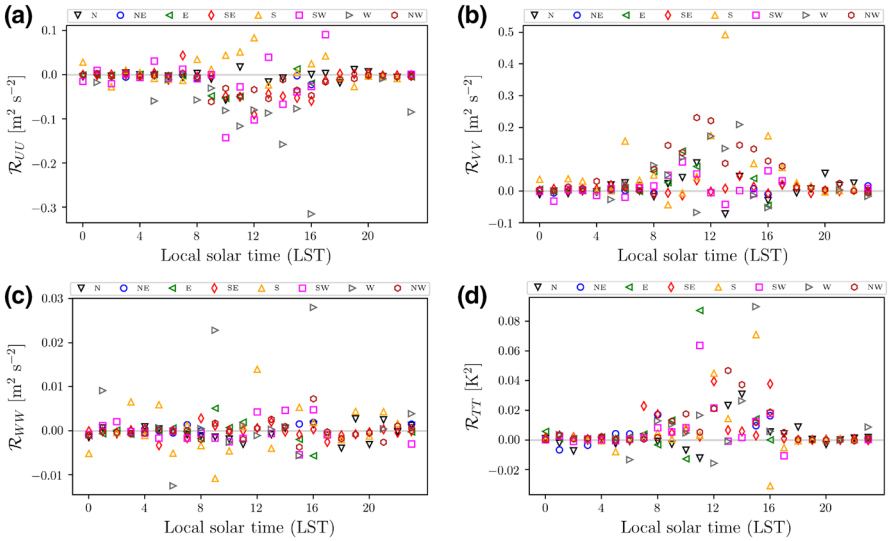

Fig. 15 Hourly symmetric autocorrelations $\mathcal{R}_{UU}$ (**a**), $\mathcal{R}_{VV}$ (**b**), $\mathcal{R}_{WW}$ (**c**), and $\mathcal{R}_{TT}$ (**d**), classified based on the roof wind angle and diurnal time

where **e** is the unit vector pointing from the street station to the roof station [1]. The autocorrelations $\mathcal{R}_{UU}$, $\mathcal{R}_{VV}$, and $\mathcal{R}_{WW}$ calculated using the data from the two weather stations should be crude estimates proportional to the true integral lengthscales that cannot be practically measured precisely. Figure 15 shows these symmetric autocorrelations and in fact these show a trend. Note that $\mathcal{R}_{UU}$ is negative due to the presence of the canyon vortex. Except for the negative sign, it can be observed that $\mathcal{R}_{UU}$ and $\mathcal{R}_{VV}$ peak during thermally unstable mid day periods. Furthermore, while R_{WW} does not peak during mid day, it is an order of magnitude smaller than $\mathcal{R}_{UU}$ and $\mathcal{R}_{VV}$. $\mathcal{R}_{TT}$ is primarily positive and also peaks during mid day, suggesting that thermal structures during heating periods have scales at least as large as the distance between the weather stations [1].

Figure 16 shows the hourly symmetric structure functions calculated using the data from roof-level and street-level weather stations. These plots depict the structure of the flow and temperature as measured by the two weather stations. The structure functions for U, V, and W components of the flow peak during the thermally unstable mid day periods, meaning the velocity differences between the two weather stations during those periods are maximized. The structure function $\mathcal{D}_{WW}$ is a factor of two lower than $\mathcal{D}_{UU}$ or $\mathcal{D}_{VV}$,

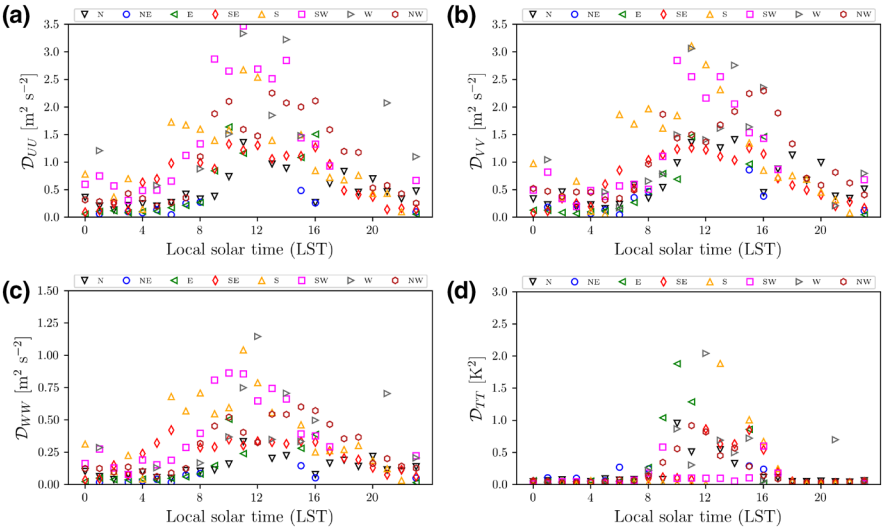

Fig. 16 Hourly symmetric structure functions $\mathcal{D}_{UU}$ (**a**), $\mathcal{D}_{VV}$ (**b**), $\mathcal{D}_{WW}$ (**c**), and $\mathcal{D}_{TT}$ (**d**), classified based on the roof wind angle and diurnal time

indicating that the velocity difference in the vertical direction is less. A similar observation can be made for the structure of temperature. Since $\mathcal{D}_{TT}$ is also maximized during mid day hours, it is speculated that temperature difference between roof and street-level weather stations is the greatest during those hours.

4.8 TANAB observations of vertical profiles of temperature and relative humidity

Figure 17 shows the vertical profiles of temperature and relative humidity (*RH*) measured using the TANAB system. Due to logistical difficulties in launching the system, only six profiles were obtained. However, these profiles were measured during different diurnal times, from the early morning to the late afternoon, in order to observe different atmospheric stability conditions. TANAB was flown up to an altitude of 40 m, weather permitting, or otherwise up to a lower altitude. Each profile was obtained in approximately 20 min where TANAB was ascended/descended twice while collecting data.

The temperature profiles show a cycle of stable–neutral–unstable–neutral conditions starting from early morning (0600 LST) and finishing at late afternoon (1600 LST). Under stable conditions, the temperature inside the canyon is lower than the temperature aloft. Under neutral conditions, the profiles approach uniform temperatures at all heights. Under unstable conditions, the temperature inside the canyon is greater than the temperature aloft. The temperatures are not corrected for the lapse rate since for the heights of interest the maximum temperature difference due to lapse rate will be significantly smaller than the range of temperature differences observed. For instance, assuming a lapse rate of 0.006 K m^{-1} [24], the temperature difference over a 25-m height interval will be only 0.15 K. The temperature profile on 15 August 2017 at 0700 LST indicates a local heating event at roof level, where solar heating increased roof level temperatures while canyon interior remained shaded without significant vertical mixing of the heated parcels of air so that temperatures above or below were not influenced.

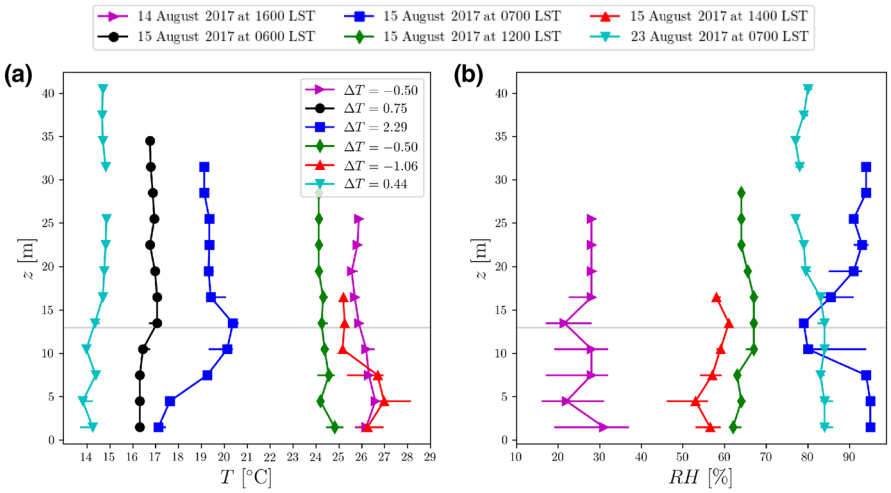

Fig. 17 Vertical profiles of **a** temperature (T) and **b** relative humidity (RH) measured using the TANAB system for selected dates and times; the building height is represented by a horizontal grey line. The markers indicate medians and the error bar represents the 25th and 75th percentiles of the sample at blocks of 3-m height intervals. Temperature gradient (ΔT) is calculated for the difference in sonic temperatures as measured by the street and roof weather stations

Profiles of the relative humidity (RH) show significant dependence on diurnal time, or equivalently thermal stability. The greatest RH is observed under thermally stable conditions during early morning, while lower RH is observed under unstable conditions during the late afternoon. Under neutral conditions, the profiles approach uniform RH at all heights. In the early morning, RH is higher within the canyon compared to RH aloft, while during the mid afternoon RH is lower inside the canyon compared to RH aloft. Similar to the temperature profile, the RH profile also shows the local heating event on 15 August 2017 at 0700 LST. This event reduced roof level RH without significant vertical mixing of the air parcels so that RH above or below were not influenced.

As tethered balloons or radiosondes tend not to be used in dense urban areas due to practical limitations [6], TANAB can potentially complement limited previous balloon observations in urban areas in the future [38, 40].

4.9 Scaling analysis

We have performed a systematic scaling analysis where the most significant correlations have been identified for each variable to be scaled using other scaling variables. The highest three correlations are listed in Tables 3, 4, and 5 with decreasing correlation coefficients (r) from high to low for each scaled variable. In addition, the fit constants (a, b) for a linear regression ($y = ax + b$) have been provided for each fit. We have attempted to find these correlations under all atmospheric conditions of wind speeds, wind directions, and thermal stabilities, using the entire dataset. It must be warned that these results only apply to this particular field campaign and cannot be extrapolated to other conditions, unless more diverse observations across different urban morphologies are conducted. In the following analysis, a significant correlation is defined with $r > 0.4$ or $r < -0.4$, i.e. significant positive and negative correlations such that $|r| > 0.4$.

Table 3 Scaling of mean vertical velocity $\overline{W}$ and friction velocity u_*

Scaled Var.	Scaling Var.								
	Var. 1			Var. 2			Var. 3		
	a	b	r	a	b	r	a	b	r
$\overline{W}_R$	$\overline{V}_R$			u_{*R}			$\overline{S}_G$		
	− 0.04	− 0.01	− 0.75	− 0.31	0.07	− 0.67	− 0.02	0.03	− 0.53
$\overline{W}_S$	$\overline{U}_S$			u_{*S}			$\overline{S}_S$		
	− 0.41	0.06	− 0.90	0.24	− 0.06	0.87	0.26	− 0.18	0.54
u_{*R}	$\overline{S}_G$			$\overline{S}_R$			$\overline{S}_S$		
	0.07	0.12	0.81	0.15	0.07	0.80	0.14	0.18	0.54
u_{*S}	$\overline{S}_S$			$\overline{S}_R$			$\overline{S}_G$		
	1.38	− 0.69	0.77	0.12	0.21	0.09	0.02	0.33	0.03

Subscripts R and S signify roof and street, respectively; constants of the linear regression $y = ax + b$ with correlation coefficient r are shown for each fit, where y is the scaled variable and x is the scaling variable. For each scaled variable, the scaling variables are ranked from highest r to lowest r

From the following discussion, it will be observed that there are suitable scaling variables for most components of momentum flux except for horizontal flux at street level. This can be attributed to the presence of unorganized and irregular turbulent motions along the street canyon axis. In addition, the horizontal heat fluxes at roof level cannot be successfully scaled, possibly due to the fact that those fluxes are highly non-local, for instance caused by passage of thermal structures over the roof. On the other hand, at street level the horizontal fluxes can be successfully scaled if they are considered normal to the canyon axis, while fluxes along the canyon axis cannot be scaled. The former can be understood as a local process, while the latter can be understood as non-local, again caused by unorganized and irregular motion of thermal structures along the canyon axis. In contrast, vertical heat fluxes scale well by local variables both at roof and street levels. This suggest that these fluxes are generated and observed locally. This interpretation is consistent with the observation of integral lengthscales and timescales in Sect. 4.6, where it was suggested the horizontal integral scales are larger compared to vertical integral scales. Finally, it can be seen that the temperature difference between urban surfaces and the adjacent atmosphere can be used to scale heat fluxes in the atmosphere, at least when they are generated locally.

Table 3 shows the scaling analysis for mean vertical velocity and friction velocity. The highest correlation for mean vertical velocity at roof level $\overline{W}_R$ is found with roof-level velocity $\overline{V}_R$ ($r = -0.75$). There is still significant correlation with roof-level friction velocity u_{*R} or the rural wind speed $\overline{S}_G$. The highest correlation for mean vertical velocity at street level $\overline{W}_S$ is found with street-level velocity $\overline{U}_S$ ($r = -0.90$). There is still significant correlation with street-level friction velocity u_{*S} or the street-level wind speed $\overline{S}_S$. These observations indicate that mean vertical motions are mostly influenced by local features of the flow, for example a building or slanted roof in the vicinity. The highest correlation for friction velocity at roof level u_{*R} is found with rural wind speed $\overline{S}_G$ ($r = 0.81$). There is still significant correlation with roof-level velocity $\overline{S}_R$ or even street-level velocity $\overline{S}_S$. The highest correlation for friction velocity at street level u_{*S} is found with street-level velocity $\overline{S}_S$ ($r = 0.77$) while no other significant correlation was found.

Table 4 Scaling of variances

Scaled Var.	Scaling Var.								
	Var. 1			Var. 2			Var. 3		
	a	b	r	a	b	r	a	b	r
$\overline{w^2}_R$	k_R			u^2_{*R}			$\overline{S}^2_G$		
	0.20	0.02	0.96	1.33	0.03	0.94	0.01	0.08	0.80
$\overline{w^2}_S$	k_S			u^2_{*S}			$\overline{S}^2_S$		
	0.51	− 0.07	1.00	0.66	0.08	1.00	1.74	− 0.76	0.90
$\overline{u^2}_R$	k_R			u^2_{*R}			$\overline{S}^2_G$		
	0.83	− 0.01	0.97	5.27	0.07	0.91	0.05	0.24	0.81
$\overline{u^2}_S$	k_S			u^2_{*S}			$\overline{S}^2_S$		
	1.46	− 0.27	1.00	1.88	0.17	0.99	4.95	− 2.23	0.89
$\overline{v^2}_R$	k_R			u^2_{*R}			$\overline{S}^2_G$		
	0.97	− 0.01	0.97	5.86	0.11	0.87	0.06	0.27	0.81
$\overline{v^2}_S$	$\overline{S}^2_G$			$\overline{V}^2_S$			$\overline{S}^2_S$		
	0.03	0.17	0.30	1.60	0.23	0.25	0.12	0.27	0.24
k_R	u^2_{*R}			$\overline{S}^2_G$			$\overline{S}^2_R$		
	6.23	0.11	0.92	0.06	0.29	0.83	0.17	0.27	0.73
k_S	u^2_{*S}			$\overline{S}^2_S$			$\overline{S}^2_R$		
	1.28	0.30	0.99	3.4	− 1.36	0.90	0.19	1.15	0.08
$\overline{t^2}_R$	$(\overline{wt}/\overline{S}_R)^2$			$(\overline{wt}/u_{*R})^2$			$(\overline{T}_{SR} - \overline{T}_R)^2$		
	48.8	0.04	0.88	0.93	0.08	0.74	0.01	0.11	0.51
$\overline{t^2}_S$	$(\overline{wt}/u_{*S})^2$			$(\overline{wt}/\overline{S}_S)^2$			$(\overline{T}_{SC} - \overline{T}_S)^2$		
	1.65	0.03	1.00	0.48	0.06	0.97	0.11	0.69	0.19

Subscripts R and S signify roof and street, respectively; $\overline{T}_{SR}$ signifies roof surface temperature, and $\overline{T}_{SC}$ signifies canyon surface temperature averaged over canyon walls and street; constants of the linear regression $y = ax + b$ with correlation coefficient r are shown for each fit, where y is the scaled variable and x is the scaling variable. For each scaled variable, the scaling variables are ranked from highest r to lowest r

Table 4 shows the scaling analysis for variances. The highest correlations for vertical velocity variances $\overline{w^2}_R$ and $\overline{w^2}_S$ at both roof and street levels are found with k_R and k_S, respectively ($r = 0.96$, $r = 1.00$). There is still significant correlation with respective friction velocities u^2_{*R} and u^2_{*S} as well as rural and local mean wind speeds $\overline{S}^2_G$ and $\overline{S}^2_S$. The highest correlations for horizontal velocity variances $\overline{u^2}_R$ and $\overline{u^2}_S$ at both roof and street levels are found with k_R and k_S, respectively ($r = 0.97$, $r = 1.00$). There is still significant correlation with respective friction velocities u^2_{*R} and u^2_{*S} as well as rural and local mean wind speeds $\overline{S}^2_G$ and $\overline{S}^2_S$. Likewise, the highest correlation for horizontal velocity variance $\overline{v^2}_R$ at roof level is found with k_R ($r = 0.97$). There is still significant correlation with friction velocity u^2_{*R} and rural mean wind speeds $\overline{S}^2_G$. However, correlations for horizontal velocity variance $\overline{v^2}_S$ at street level are very weak at best with rural mean wind speed $\overline{S}^2_G$ ($r = 0.30$). The highest correlation for TKE k_R at roof level is with local friction velocity u^2_{*R} ($r = 0.92$), while other significant correlations are found with rural and local wind speeds $\overline{S}^2_G$ and $\overline{S}^2_R$. The highest correlation for TKE k_S at street level is with local

Table 5 Scaling of covariances, or equivalently the Reynolds stresses and the turbulence kinematic heat fluxes

Scaled Var.	Scaling Var.								
	Var. 1			Var. 2			Var. 3		
	a	b	r	a	b	r	a	b	r
$\overline{uv}_R$	k_R			$\overline{S}_G^2$			u_{*R}^2		
	0.09	− 0.02	0.46	0.01	0.01	0.43	0.35	0.02	0.25
$\overline{uv}_S$	k_S			u_{*S}^2			$\overline{S}_S^2$		
	0.01	0.01	0.13	0.01	0.01	0.09	0.02	0.00	0.08
$\overline{uw}_R$	u_{*R}^2			k_R			$\overline{S}_G^2$		
	0.46	− 0.01	0.52	0.06	− 0.01	0.48	0.01	0.01	0.35
$\overline{uw}_S$	u_{*S}^2			k_S			$\overline{S}_S^2$		
	− 0.99	0.03	− 0.99	− 0.76	0.25	− 0.98	− 2.59	1.28	− 0.89
$\overline{vw}_R$	u_{*R}^2			$\overline{S}_G^2$			k_R		
	− 0.68	0.02	− 0.70	− 0.01	− 0.01	− 0.67	− 0.09	0.02	− 0.65
$\overline{vw}_S$	k_S			u_{*S}^2			$\overline{S}_S^2$		
	0.01	0.01	0.14	0.01	0.02	0.12	0.03	0.00	0.11
$\overline{ut}_R$	$\overline{S}_G(\overline{T}_{SR} - \overline{T}_R)$			$u_{*R}(\overline{T}_{SR} - \overline{T}_R)$			$\overline{S}_R(\overline{T}_{SR} - \overline{T}_R)$		
	0.00	0.01	0.04	0.01	0.01	0.03	0.00	0.00	0.00
$\overline{ut}_S$	$u_{*S}(\overline{T}_{SC} - \overline{T}_S)$			$\overline{S}_S(\overline{T}_{SC} - \overline{T}_S)$			$\overline{S}_G(\overline{T}_{SC} - \overline{T}_S)$		
	1.17	0.56	0.63	1.47	0.43	0.53	0.25	0.72	0.20
$\overline{vt}_R$	$\overline{S}_G(\overline{T}_{SR} - \overline{T}_R)$			$u_{*R}(\overline{T}_{SR} - \overline{T}_R)$			$\overline{S}_R(\overline{T}_{SR} - \overline{T}_R)$		
	− 0.01	− 0.02	− 0.11	− 0.01	− 0.03	− 0.08	− 0.01	0.03	− 0.05
$\overline{vt}_S$	$u_{*S}(\overline{T}_{SC} - \overline{T}_S)$			$\overline{S}_S(\overline{T}_{SC} - \overline{T}_S)$			$\overline{S}_G(\overline{T}_{SC} - \overline{T}_S)$		
	− 0.01	0.04	− 0.20	− 0.01	0.04	− 0.02	− 0.01	0.04	− 0.02
$\overline{wt}_R$	$u_{*R}(\overline{T}_{SR} - \overline{T}_R)$			$\overline{S}_R(\overline{T}_{SR} - \overline{T}_R)$			$\overline{S}_G(\overline{T}_{SR} - \overline{T}_R)$		
	0.02	0.03	0.41	0.01	0.03	0.41	0.01	0.03	0.38
$\overline{wt}_S$	$u_{*S}(\overline{T}_{SC} - \overline{T}_S)$			$\overline{S}_S(\overline{T}_{SC} - \overline{T}_S)$			$\overline{S}_G(\overline{T}_{SC} - \overline{T}_S)$		
	− 0.78	− 0.37	− 0.62	− 0.97	− 0.28	− 0.52	− 0.16	− 0.48	− 0.20

Subscripts R and S signify roof and street, respectively; $\overline{T}_{SR}$ signifies roof surface temperature, and $\overline{T}_{SC}$ signifies canyon surface temperature averaged over canyon walls and street; constants of the linear regression $y = ax + b$ with correlation coefficient r are shown for each fit, where y is the scaled variable and x is the scaling variable. For each scaled variable, the scaling variables are ranked from highest r to lowest r

friction velocity u_{*S}^2 ($r = 0.99$), while only another significant correlation is found with local wind speed $\overline{S}_S$. The highest correlation for temperature variance $\overline{t^2}_R$ at roof level is with $(\overline{wt}/\overline{S}_R)^2$ ($r = 0.88$), while other significant correlations are found with $(\overline{wt}/u_{*R})^2$ and $(\overline{T}_{SR} - \overline{T}_R)^2$, where $\overline{T}_{SR}$ is roof surface temperature measured with the thermal camera. The highest correlation for temperature variance $\overline{t^2}_S$ at street level is with $(\overline{wt}/u_{*S})^2$ ($r = 1.00$), while only one other significant correlation is found with $(\overline{wt}/\overline{S}_S)^2$. In this case, there is a weak correlation with $(\overline{T}_{SC} - \overline{T}_S)^2$, where $\overline{T}_{SC}$ is canyon mean surface temperature. From the discussion above, it appears that reliable scaling variables can be found for most scaled

variances, except for $\overline{v^2}_S$. This is justified by the hypothesis that the along-canyon turbulent motions are unorganized and irregular. In addition, it can be observed that the temperature difference between urban surfaces and the adjacent atmosphere can be used to scale temperature variances in the atmosphere locally, particularly more successfully at roof level.

Table 5 shows the scaling analysis for covariances or alternatively turbulence kinematic fluxes. In general, most correlations observed are weaker than those observed for mean velocities and variances. The highest correlation for horizontal momentum flux $\overline{uv}_R$ at roof level is found with k_R ($r = 0.46$), followed by mean rural wind speed $\overline{S}^2_G$. No significant correlation is observed for horizontal momentum flux $\overline{uv}_S$ at street level. The highest correlation for vertical momentum flux $\overline{uw}_R$ is observed with local friction velocity u^2_{*R} ($r = 0.52$), followed by local TKE k_R. The highest correlation for vertical momentum flux $\overline{uw}_S$ at street level is observed with local friction velocity u^2_{*S} ($r = -0.99$), while other significant correlations exist with local TKE k_S and mean local wind speed $\overline{S}^2_S$. The highest correlation for vertical momentum flux $\overline{vw}_R$ at roof level is observed with local friction velocity u^2_{*R} ($r = -0.70$), while other significant correlations are observed with rural mean wind speed $\overline{S}^2_G$ and local TKE k_R. There is no significant correlation for vertical momentum flux $\overline{vw}_S$ at street level. The horizontal heat flux $\overline{ut}_R$ at roof level is not correlated significantly with any scaling variable. The horizontal heat flux $\overline{ut}_S$ at street level is most significantly correlated with $u_{*S}(\overline{T}_{SC} - \overline{T}_S)$ ($r = 0.63$) and $\overline{S}_S(\overline{T}_{SC} - \overline{T}_S)$ ($r = 0.53$). The horizontal heat fluxes $\overline{vt}_R$ and $\overline{vt}_S$ are not correlated significantly with any scaling variable. Significant correlations are found for vertical heat flux $\overline{wt}_R$ at roof level with $u_{*R}(\overline{T}_{SR} - \overline{T}_R)$ and $\overline{S}_R(\overline{T}_{SR} - \overline{T}_R)$ ($r = 0.41$, $r = 0.41$). Significant correlations are found for vertical heat flux $\overline{wt}_S$ at street level with $u_{*S}(\overline{T}_{SC} - \overline{T}_S)$ ($r = -0.62$) and $\overline{S}_S(\overline{T}_{SC} - \overline{T}_S)$ ($r = -0.52$).

5 Conclusions and future work

The dynamics of the urban microclimate under a comprehensive set of wind directions, wind speeds, and thermal stability conditions were studied in a field campaign held in Guelph, Ontario, Canada, from 13th to 25th of August 2017. The urban site was a quasi-two-dimensional canyon with unit canyon aspect ratio. Two weather stations were installed to acquire wind speed, wind direction, and temperature continuously: one at roof level and the other at street level. A Tethered And Navigated Air Blimp (TANAB) was used to obtain vertical profiles of temperature and relative humidity (*RH*) for selected times. Thermal imaging was used to measure urban surface temperatures, both within the canyon and on the roof for selected times. In addition, microclimate data was accessed for a rural weather station outside the urban area.

Thermal stability and inertial effects were observed to be dependent on the diurnal cycle. The thermal stability cycled from stable conditions at night to unstable conditions in the mid afternoon. Wind speeds were the highest during the mid afternoon periods. The urban heat island (UHI) intensity was quantified. Local mean vertical air motions were observed at roof-level and street-level weather stations, likely influenced by wind direction, wind speed, and nearby buildings or building features.

Turbulence statistics were analyzed as functions of wind direction at roof level, diurnal time, wind speed, and thermal stability. The statistics involved calculation of variances, covariances, integral timescales, integral lengthscales, two-point correlations, and structure functions. The statistics were observed to be highly dependent on wind

direction at roof level, diurnal time, wind speed, and thermal stability. Turbulence statistics in the vertical direction were observed to be influenced by local conditions and characterized by small integral lengthscales and short integral timescales. On the other hand, turbulence statistics in the horizontal direction were observed to be influenced by non-local conditions and characterized by larger integral lengthscales and longer integral timescales. The integral scales varied from roof level to street level but not so much as they varied from horizontal to vertical directions. The horizontal components of Reynolds stresses and heat fluxes were observed to be just as high as the vertical components, suggesting that such fluxes could influence the canyon microclimate if sufficient flux gradients existed in the horizontal direction. In addition, local inhomogeneity was observed in the turbulence heat flux, indicating that turbulence heat flow had preferred horizontal directions to exchange.

A rigorous scaling analysis was performed to find the most significant correlation coefficients $|r| > 0.4$ between mean or turbulence quantities and other known flow conditions either at the rural station or locally (i.e. roof-level or street-level weather stations). For momentum related quantities, the rural station provided acceptable scaling for various quantities, while local variables such as turbulence kinetic energy (TKE) or friction velocity also provided significant correlation coefficients. Momentum variances were scaled well, except for the along-canyon variance at street level, likely due to unpredictable and non-local influence of large scale, unorganized, and irregular flow along the canyon. Reynolds stresses still scaled but to a lesser extent compared to momentum variances. The vertical momentum fluxes were scaled more successfully while the horizontal fluxes, especially at street level, did not scale well. For heat related quantities, the local variables such as friction velocity, mean velocity, local turbulence kinematic heat flux, and temperature difference between surfaces and the atmosphere, provided acceptable scaling. Scaling was more successful for temperature variance compared to turbulence kinematic heat flux. Also scaling of the turbulence kinematic heat flux was more successful in the vertical direction using local conditions, as opposed to the horizontal directions, likely due to the passage of non-local thermal structures over the measurement areas. It appears that surface temperature mapping and the surface-atmosphere temperature difference are useful for heat flux scaling in the vertical, and possibly horizontal, directions.

This study may support more accurate simulation, model design, and development of urban areas with better air quality and climate control within urban canyons. Future work shall involve longer term observations to investigate seasonal dependence of parameters studied. In addition, more weather stations can be installed with added resolution in the vertical and horizontal directions so that turbulence flux gradients can be adequately measured to inform future urban canopy model development. This approach shall also be extended to three-dimensional canyons with heterogeneous urban morphology so that effects of intersections and deep canyons can also be observed. These measurements were performed for one specific urban configuration and future work should aim to cover the role of morphology as well. Other rigorous analysis using other metrics for characterizing street canyon thermal stability conditions is also needed.

Acknowledgements The authors thank Physical Resources staff members at the University of Guelph, in particular Steve Nyman and Chris Duiker, for assisting with the campaign logistics. The authors also thank Health and Safety staff members at the University of Guelph, in particular Manuela Racki and Jeffrey Dafoe, for assisting with safety inspections required to authorize the campaign. The authors appreciate the assistance of Joanne Ryks, Ryan Smith, and Stephen Stajkowski with the logistics of the field campaign.

Funding Financial support for this project was provided by the Undergraduate Research Awards (URA) program from the University of Guelph and the Discovery Grant program from Natural Sciences and Engineering Research Council (NSERC) of Canada (Grant No. 401231).

References

1. Aliabadi AA (2018) Theory and applications of turbulence: a fundamental approach for scientists and engineers. Amir A. Aliabadi Publications, Guelph, ON
2. Aliabadi AA, Staebler RM, Liu M, Herber A (2016) Characterization and parametrization of Reynolds stress and turbulent heat flux in the stably-stratified lower Arctic troposphere using aircraft measurements. Boundary-Layer Meteorol 161(1):99–126
3. Aliabadi AA, Krayenhoff ES, Nazarian N, Chew LW, Armstrong PR, Afshari A, Norford LK (2017) Effects of roof edge roughness on air temperature and pollutant concentration in urban canyons. Boundary-Layer Meteorol 164(2):249–279
4. Arnfield AJ (2003) Two decades of urban climate research: a review of turbulence, exchanges of energy and water, and the urban heat island. Int J Climatol 23(1):1–26
5. Balogun AA, Tomlin AS, Wood CR, Barlow JF, Belcher SE, Smalley RJ, Lingard JJN, Arnold SJ, Dobre A, Robins AG, Martin D, Shallcross DW (2010) In-street wind direction variability in the vicinity of a busy intersection in central London. Boundary-Layer Meteorol 136(3):489–513
6. Barlow JF, Halios CH, Lane SE, Wood CR (2015) Observations of urban boundary layer structure during a strong urban heat island event. Environ Fluid Mech 15(2):373–398
7. Blackman K, Perret L, Savory E, Piquet T (2015) Field and wind tunnel modeling of an idealized street canyon flow. Atmos Environ 106:139–153
8. Cheng WC, Porté-Agel F (2015) Adjustment of turbulent boundary-layer flow to idealized urban surfaces: a large-eddy simulation study. Boundary-Layer Meteorol 155(2):249–270
9. Chew LW, Nazarian N, Norford L (2017) Pedestrian-level urban wind flow enhancement with wind catchers. Atmosphere (Basel) 8(159):1–22
10. Coutts AM, White EC, Tapper NJ, Beringer J, Livesley SJ (2016) Temperature and human thermal comfort effects of street trees across three contrasting street canyon environments. Theor Appl Climatol 124(1):55–68
11. Eliasson I, Offerle B, Grimmond CSB, Lindqvist S (2006) Wind fields and turbulence statistics in an urban street canyon. Atmos Environ 40(1):1–16
12. Giometto MG, Christen A, Meneveau C, Fang J, Krafczyk M, Parlange MB (2016) Spatial characteristics of roughness sublayer mean flow and turbulence over a realistic urban surface. Boundary-Layer Meteorol 160(3):425–452
13. Girard P (2016) Validation partielle et développement d'un modèle de microclimat urbain. Master's thesis, Laval University
14. Graf A, van de Boer A, Moene A, Vereecken H (2014) Intercomparison of methods for the simultaneous estimation of zero-plane displacement and aerodynamic roughness length from single-level eddy-covariance data. Boundary-Layer Meteorol 151(2):373–387
15. Hu XM, Xue M, Klein PM, Illston BG, Chen S (2016) Analysis of urban effects in Oklahoma city using a dense surface observing network. J Appl Meteorol Clim 55(3):723–741
16. Inagaki A, Kanda M (2008) Turbulent flow similarity over an array of cubes in near-neutrally stratified atmospheric flow. J Fluid Mech 615:101–120
17. Inagaki A, Kanda M (2010) Organized structure of active turbulence over an array of cubes within the logarithmic layer of atmospheric flow. Boundary-Layer Meteorol 135(2):209–228
18. Jamei E, Rajagopalan P, Seyedmahmoudian M, Jamei Y (2016) Review on the impact of urban geometry and pedestrian level greening on outdoor thermal comfort. Renew Sust Energ Rev 54:1002–1017
19. Kastner-Klein P, Berkowicz R, Britter R (2004) The influence of street architecture on flow and dispersion in street canyons. Meteorol Atmos Phys 87(1):121–131
20. Kellnerová R, Kukačka L, Jurčáková K, Uruba V, Jaňour Z (2012) PIV measurement of turbulent flow within a street canyon: detection of coherent motion. J Wind Eng Ind Aerodyn 104–106:302–313
21. Klein P, Clark JV (2007) Flow variability in a North American downtown street canyon. J Appl Meteorol Clim 46:851–877
22. Klein PM, Galvez JM (2015) Flow and turbulence characteristics in a suburban street canyon. Environ Fluid Mech 15(2):419–438

23. Krayenhoff ES, Voogt JA (2007) A microscale three-dimensional urban energy balance model for studying surface temperatures. Boundary-Layer Meteorol 123(3):433–461
24. Krayenhoff ES, Voogt JA (2010) Impacts of urban albedo increase on local air temperature at daily-annual time scales: model results and synthesis of previous work. J Appl Meteorol Clim 49:1634–1648
25. Krayenhoff ES, Santiago JL, Martilli A, Christen A, Oke TR (2015) Parametrization of drag and turbulence for urban neighbourhoods with trees. Boundary-Layer Meteorol 156(2):157–189
26. Li XX, Britter RE, Koh TY, Norford LK, Liu CH, Entekhabi D, Leung DYC (2010) Large-eddy simulation of flow and pollutant transport in urban street canyons with ground heating. Boundary-Layer Meteorol 137(2):187–204
27. Li XX, Britter RE, Norford LK (2015) Transport processes in and above two-dimensional urban street canyons under different stratification conditions: results from numerical simulation. Environ Fluid Mech 15(2):399–417
28. Louka P, Belcher SE, Harrison RG (2000) Coupling between air flow in streets and the well-developed boundary layer aloft. Atmos Environ 34(16):2613–2621
29. Nakamura Y, Oke TR (1988) Wind, temperature and stability conditions in an east–west oriented urban canyon. Atmos Environ 22(12):2691–2700
30. Nazarian N, Kleissl J (2016) Realistic solar heating in urban areas: air exchange and street-canyon ventilation. Build Environ 95:75–93
31. Nazarian N, Martilli A, Kleissl J (2018) Impacts of realistic urban heating, part I: spatial variability of mean flow, turbulent exchange and pollutant dispersion. Boundary-Layer Meteorol 166(3):367–393
32. Nelson MA, Pardyjak ER, Brown MJ, Klewicki JC (2007) Properties of the wind field within the Oklahoma City Park Avenue street canyon. Part II: spectra, cospectra, and quadrant analyses. J Appl Meteorol Clim 46(12):2055–2073
33. Nelson MA, Pardyjak ER, Klewicki JC, Pol SU, Brown MJ (2007) Properties of the wind field within the Oklahoma City Park Avenue street canyon. Part I: mean flow and turbulence statistics. J Appl Meteorol Clim 46(12):2038–2054
34. Offerle B, Eliasson I, Grimmond CSB, Holmer B (2007) Surface heating in relation to air temperature, wind and turbulence in an urban street canyon. Boundary-Layer Meteorol 122(2):273–292
35. Ohya Y (2001) Wind-tunnel study of atmospheric stable boundary layers over a rough surface. Boundary-Layer Meteorol 98(1):57–82
36. Oke TR (1988) Street design and urban canopy layer climate. Energy Build 11(1):103–113
37. Patton EG, Sullivan PP, Shaw RH, Finnigan JJ, Weil JC (2016) Atmospheric stability influences on coupled boundary layer and canopy turbulence. J Atmos Sci 73(4):1621–1647
38. Ramamurthy P, Pardyjak ER, Klewicki JC (2007) Observations of the effects of atmospheric stability on turbulence statistics deep within an urban street canyon. J Appl Meteorol Clim 46(12):2074–2085
39. Raupach MR, Thom AS, Edwards I (1980) A wind-tunnel study of turbulent flow close to regularly arrayed rough surfaces. Boundary-Layer Meteorol 18(4):373–397
40. Rotach MW, Vogt R, Bernhofer C, Batchvarova E, Christen A, Clappier A, Feddersen B, Gryning SE, Martucci G, Mayer H, Mitev V, Oke TR, Parlow E, Richner H, Roth M, Roulet YA, Ruffieux D, Salmond JA, Schatzmann M, Voogt JA (2005) BUBBLE-an urban boundary layer meteorology project. Theor Appl Climatol 81(3):231–261
41. Saathoff P, Gupta A, Stathopoulos T, Lazure L (2009) Contamination of fresh air intakes due to downwash from a rooftop structure. J Air Waste Manage Assoc 59(3):343–353
42. Santamouris M (ed) (2006) Environmental design of urban buildings: an integrated approach. Earthscan, London
43. Santamouris M, Papanikolaou N, Koronakis I, Livada I, Asimakopoulos D (1999) Thermal and air flow characteristics in a deep pedestrian canyon under hot weather conditions. Atmos Environ 33(27):4503–4521
44. Savory E, Perret L, Rivet C (2013) Modelling considerations for examining the mean and unsteady flow in a simple urban-type street canyon. Meteorol Atmos Phys 121(1):1–16
45. Takimoto H, Sato A, Barlow JF, Moriwaki R, Inagaki A, Onomura S, Kanda M (2011) Particle image velocimetry measurements of turbulent flow within outdoor and indoor urban scale models and flushing motions in urban canopy layers. Boundary-Layer Meteorol 140(2):295–314
46. Taylor GI (1938) The spectrum of turbulence. Proc R Soc Lond A 164:476–490
47. van der Hoven I (1957) Power spectrum of horizontal wind speed in the frequency range from 0.0007 to 900 cycles per hour. J Meteorol 14(2):160–164
48. Willis GE, Deardorff JW (1976) On the use of Taylor's translation hypothesis for diffusion in the mixed layer. Q J R Meteorol Soc 102:817–822
49. Zajic D, Fernando HJS, Calhoun R, Princevac M, Brown MJ, Pardyjak ER (2011) Flow and turbulence in an urban canyon. J Appl Meteorol Clim 50(1):203–223